(2)

NAVAL POSTGRADUATE SCHOOL

Monterey, California

THESIS

DEVELOPMENT OF A SYSTEM FOR ACOUSTIC MEASUREMENTS OF BISTATIC TARGET STRENGTHS

by

GLENN R. SNYDER

September 1988

Thesis Advisors: J. V. Sanders
A. B. Coppens

Unclassified

Security Classification of this page

REPORT DOCUMENTATION PAGE

1a Report Security Classification: Unclassified	1b Restrictive Markings
2a Security Classification Authority	3 Distribution Availability of Report: Approved for public release; distribution is unlimited.
2b Declassification/Downgrading Schedule	
4 Performing Organization Report Number(s)	5 Monitoring Organization Report Number(s)
6a Name of Performing Organization: Naval Postgraduate School; 6b Office Symbol (If Applicable): 33	7a Name of Monitoring Organization: Naval Postgraduate School
6c Address (city, state, and ZIP code): Monterey, CA 93943-5000	7b Address (city, state, and ZIP code): Monterey, CA 93943-5000
8a Name of Funding/Sponsoring Organization; 8b Office Symbol (If Applicable)	9 Procurement Instrument Identification Number
8c Address (city, state, and ZIP code)	10 Source of Funding Numbers: Program Element Number; Project No; Task No; Work Unit Accession No

11 Title (Include Security Classification): DEVELOPMENT OF A SYSTEM FOR ACOUSTIC MEASUREMENTS OF BISTATIC TARGET STRENGTHS

12 Personal Author(s): Glenn R. Snyder

13a Type of Report	13b Time Covered	14 Date of Report (year, month,day)	15 Page Count
Master's Thesis	From To	September 1988	90

16 Supplementary Notation: The views expressed in this thesis are those of the author and do not reflect the official policy or position of the Department of Defense or the U.S. Government.

17 Cosati Codes			18 Subject Terms (continue on reverse if necessary and identify by block number)
Field	Group	Subgroup	BistaticTarget Strength, Sound Scattering,

19 Abstract (continue on reverse if necessary and identify by block number)

A digital data acquisition system was implemented for the study and collection of scattered waveforms from various objects. Reflected waveforms were extracted from interference with other signals by a simple subtraction technique. Backscattered and bistatic reflections were observed and and recorded. Various effects on scattered waveforms, including target composition, pulse length, and frequency, were experimentally observed. Bistatic scattering results from a styrofoam sphere at a ka value of 10 were in agreement with theoretical predictions for a rigid sphere. Bistatically measured data at 70 kHz from a styrofoam cylinder of length 20 cm and diameter 2.5 cm followed a trend for bistatic angles up to 150 degrees but became amorphous as the bistatic angle approached 180 degrees.

20 Distribution/Availability of Abstract	21 Abstract Security Classification	
[X] unclassified/unlimited [ ] same as report [ ] DTIC users	Unclassified	
22a Name of Responsible Individual: James V. Sanders	22b Telephone (Include Area code): (408) 646-2931	22c Office Symbol: 61Sd

DD FORM 1473, 84 MAR — 83 APR edition may be used until exhausted; All other editions are obsolete

security classification of this page: Unclassified

Approved for public release; distribution is unlimited.

DEVELOPMENT OF A SYSTEM FOR ACOUSTIC MEASUREMENTS OF BISTATIC TARGET STRENGTHS

by

Glenn R. Snyder
Lieutenant, United States Navy
B.S., United States Naval Academy, 1982

Submitted in partial fulfillment of the
requirements for the degree of

MASTER OF SCIENCE IN PHYSICS

from the

NAVAL POSTGRADUATE SCHOOL
September 1988

Author: _____
Glenn R. Snyder

Approved By: _____
James V. Sanders, Co-Advisor

_____
Alan B. Coppens, Co-Advisor

_____
Karlheinz E. Wohler, Chairman, Department of Physics

_____
Gordon E. Schacher, Dean of Science and Engineering

ABSTRACT

A digital data acquisition system was implemented for the study and collection of scattered waveforms from various simple objects. Reflected waveforms were extracted from interference with other signals by a simple subtraction technique. Backscattered and bistatic reflections were observed and recorded. Various effects on scattered waveforms, including target composition, pulse length, and frequency, were experimentally observed. Bistatic scattering results from a stryofoam sphere at a ka value of 10 were in agreement with theoretical predictions for a rigid sphere. Bistatically measured data at 70 kHz from a styrofoam cylinder of length 20 cm and diameter 2.5 cm followed a trend for bistatic angles up to 150 degrees but became amorphous as the bistatic angle approached 180 degrees.

TABLE OF CONTENTS

LIST OF FIGURES

I. INTRODUCTION

Any object with a characteristic impedance different from the surrounding fluid will affect an acoustic wave impinging on it. The wave will be transmitted through the object and scattered from it. Flexural waves, compressional waves, and creeping waves are examples of some of the possible scattering and reflection mechanisms [Ref. 1:p. 301]. The "characteristic impedance" equals the density of a material multiplied by the speed of sound in the material. It is one measure used to calculate reflection factors for pressure waves. Other properties that affect the scattering properties of an object include frequency, shape of the object, and pulse length.

Ever since the development of the submarine as an important force in naval warfare, much effort has been directed to improving their detection. The same holds true for the submarine detecting of surface ships or other submarines. The knowledge required for detection include knowing the source level of the target, propagation loss, noise level , and lastly target strength, the subject of this paper. These parameters are used in the well-known sonar equations [Ref. 2:p. 411]. Target strength, TS, as used in the sonar equations is defined as:

$$TS = 10 \log \frac{I_r}{I_o} \qquad (1)$$

where I_r is the reflected intensity one meter from the acoustic center of the target and I_o is the incident intensity at the target without the presence of the target. This equation is general, giving no stipulation as to the direction of the reflected intensity. Typically, signals in active sonar are sent and recevied by the same platform, thus the most common geometry and ,therefore, the most studied, is the

backscattered monostatic case where the reflected intensity is measured in the direction back toward the source. Measurement along any other direction constitutes a bistatic geometry. Relatively little effort has been given to the study of bistatic target strength until recently when the bistatic geometry was recognized as a potential method for improving underwater detection of submerged targets. Figures 1 and 2 illustrate the monostatic and bistatic geometries.

Figure 1. Backscattered Monostatic Geometry

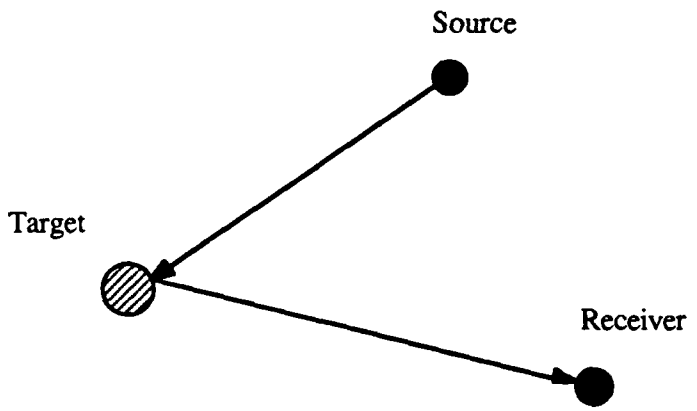

Figure 2. Bistatic Geometry

Some work has been done in the radar community on estimating the bistatic radar cross-section of objects. Crispin and Siegel [Ref. 3:p. 156] present a theorem for the approximation of radar bistatic cross-section:

> In the limit of vanishing wavelength, the bistatic cross-section for transmitter direction $\hat{k}$ and receiver $\hat{n}$ is equal to the monostatic cross-section for the transmitter-receiver direction $\hat{k} + \hat{n}$ with $\hat{k} \neq \hat{n}$ for bodies that are sufficiently smooth.

(Figure 3 illustrates the geometry as stated in the theorem.)

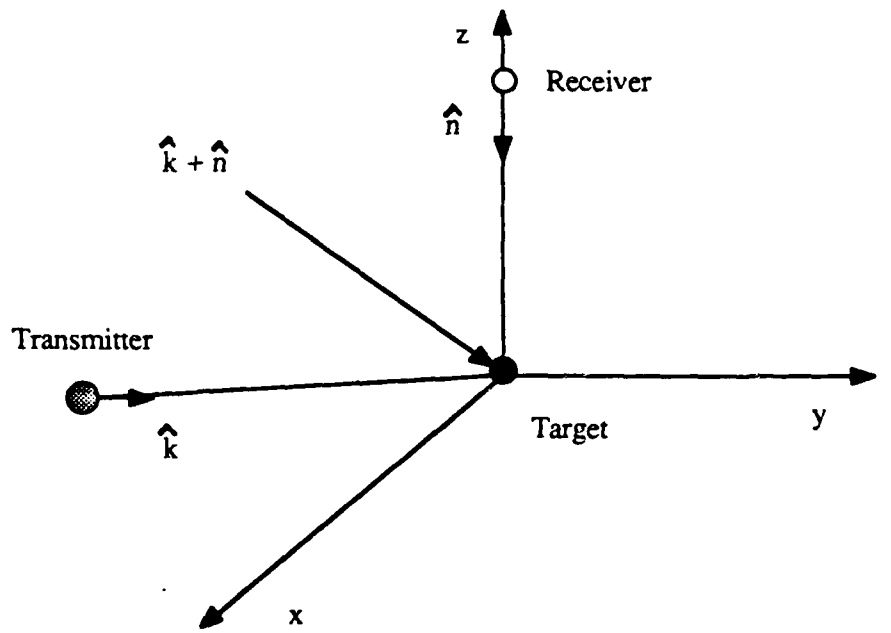

Figure 3. Radar Bistatic Cross-Section Theorem Geometry

Their bistatic theorem has its limitations when applied to complex shapes; The bistatic cross-section can be greater or less than the monostatic case due to structurally-related interferences. Another limitation is the size of the target with respect to the incident wavelength. Spheres were analyzed using various ka values

where where a is the radius of the sphere and k is the wave number. It was found that the theorem held more closely for higher ka values, but in all cases the theorem sharply deviated from experiment as the bistatic angle approached 180 degrees. As an illustrative example, they presented data on a jet aircraft and a ballistic-missile shape [Ref. 3:p. 174-177]. Data were in fairly good agreement with their theorem as long as the bistatic angle did not get too large.

In transition from the radar community to underwater acoustics, Urick [Ref. 1:p. 302] implied that the bistatic radar cross-section theorem might apply in a underwater condition, in which case the bistatic target strength was equal to the monostatic target strength taken at the bisector of the bistatic angle. Urick emphasized there was a lack of data to prove or disprove such a theory. It would be very convenient if such a theorem existed since there is plentiful target strength data for monostatic geometries. Whether or not the high frequency limitations of such a theorem would preclude its tactical use is another question.

The interest in bistatic target strength has been generated by the possibility of increasing detection of submerged and surface units using this technique. For example, one can easily visualize having a surface ship using its active sonar while a submerged submarine, using passive sonar, listens for reflections off enemy forces.

There are several advantages and disadvantages to bistatic employment. Several ideas now discussed were taken from Harvey [Ref. 4] who gave a thorough discussion on using bistatic employment as a tactical tool in naval warfare. The major advantages include the ability to maintain a track of the enemy force using passive sonar and the increased amount of data available to detect and classify targets. All units besides the active unit can be passive, thereby hampering own-ship detection. Detecting bistatic reflections, as well as backscattered reflections,

from a target increases the data available for detection and classification of the target. The greatest difficulty using a bistatic geometry is the high positional accuracy required between the pinger and the listener. This requires prior planning for use with surface ships and submarines since they do not normally have continuous open communication with each other. Another difficulty is the distinguishing of backscattered reflections from bistatic reflections. It may turn out that the advantages do not outweigh the disadvantages and the whole idea will prove infeasible.

II. TARGET STRENGTH

A. INTRODUCTION

This chapter presents some definitions and background knowledge essential in preparation for experimentation. Some concepts are rather simple but are included for completeness.

B. DEFINITION

The definition of target strength has already been given, equation (1). However, there are several aspects of the definition that warrant clarification. First, all measurements are taken in the far field of the target. The far field is where the pressure reflected from an object exhibits a 1/r relationship [Ref. 2:p. 178]. For example, pressure measurements taken one meter from the hull of a large ship would certainly be in the near field, so intensity is measured in the far field at ranges of hundreds of meters and then extrapolated back to one meter for use in the target strength calculations.

The next question concerns the defintion of the acoustic center. Very rarely are we able to know the location of a target's acoustic center. The acoustic center is the point from which sound appears to radiate. It may be anywhere around the target, and may lie outside the shape itself. It may also change with the aspect of the target relative to the receiver. Exact location of the target's acoustic center is ignored in field measurements, and the geometrical center is used. When measuring pressure at hundreds of meters, a few meters error in determination accounted for by the acoustic center will not produce a large discrepancy.

C. SPHERICAL WAVES

For a distant source, to a good approximation, the wave will appear locally as a plane wave as it encounters the target. Consider an omnidirectional point source: Spherically diverging waves are emitted and the pressure amplitude and phase is dependent only on the distance r from the acoustic center of the source. An outwardly travelling spherical wave can be represented by

$$P(r) = \frac{A}{r} e^{j(wt - kr)} \qquad (2)$$

A = pressure amplitude at one meter
r = distance from point source
w = angular frequency of signal
k = wave propagation number

When the radius of curvature of the wave front is large compared to the biggest dimension of the target, the spherical wave can be treated as a plane wave.

Plane waves are assurred when the dimensions of a target are small compared to the source-target distance. One of the goals of small-scale experiments is the application of the results to oceanic situations, therefore there is a concern about the approximation of plane waves ensonifying a target in a small laboratory tank.

The geometrical constraints of the water tank limits target-source-receiver distances. With small distances between source and receiver and big targets, a plane wave may not be a good approximation. Another factor that influences the plane wave approximation is the directionality of the source. It is difficult to achieve omnidirectional behavior from a finite source and it is impossible if the frequency is high. Beam patterns are formed with energy emitted in preferred directions. If

the target subtends an angle greater than the beamwidth, the pressure amplitude will not be the same for all points on the target.

Plane waves also have properties that make target strength calculations simple to handle. The intensity can be equated to the root-mean-square pressure amplitude squared divided by the characteristic impedance [Ref. 2:p. 111]. Since hydrophones measure pressure via a sensitivity factor, the output voltage they produce can be directly related to intensity.

D. WAVEFORM EFFECTS

There are several factors to consider in the measurement and collection of reflected waveforms from objects. Some are listed below and each will cause the reflected waveform to differ from the incident waveform.

- target composition
- target shape
- pulse length
- resonance effects

For the reflected waveform to be identical of the incident waveform, a planar rigid boundary must be encountered. For more complicated targets, some of the incident energy will be transmitted into the body and eventually reradiated and different areas of the target may reflect in such a way to cause mutual interference. Many objects have resonances, at which the target will store some of the incident energy and reradiate it at a later time causing interference effects. Theoretical and experimental results show that for short pulse lengths, reflections are nearly independent of target composition and are almost identical to the incident pulse [Ref. 5,6,7] while for longer pulses the reflected waveform changes drastically depending on the composition and shape of the target.

E. EXPERIMENTAL MEASUREMENT

While conducting the literature search, it was interesting to note how the pressure amplitude of the reflected wave was measured. As stated before, hydrophones give a voltage that is representative of pressure and this can be equated to intensity. The problem lies in the fact that the reflected waveform, in most cases, is not identical to that of the incident signal. The experimenter has to specify what is measured and what kind of pulse is being used. Response can be catagorized as transient or steady-state. Steady-state implies that the whole target has been ensonified by the incident pulse allowing for all portions of the target to contribute to the reflection and for any resonances to become fully excited. In this case, the return will be a combination of all possible reflection paths and modes. A transient response simply is not in the steady-state. To give an idea of measurement used, the following are quoted from two published articles:

> ...five cycles of the sine wave located at a position in the pulse judged to be a true representation of the steady state. The average of the ten peak values so obtained gave the peak pressure amplitude [Ref. 7]

> After amplification, the amplitude of the back-scattered signal is measured with a peak detector [Ref. 8].

The main point is that for reflected waveforms, not similiar in shape to the incident waveform, some subjective determination is required. Estimation of the steady-state must be made or some definite parameter has to be selected such as peak amplitude or total energy. In any case, an unique way to convert the amplitude measurements to an intensity level is not achievable. Add to this the fact that the reflected waveform will be different for different target orientations and frequencies, and the problem of translating measurements into an intensity level to calculate a target strength becomes complicated.

There presently exists a Target Strength Standardization Program [Ref. 9] which was assigned the task of finding some standard measure of target strength independent of signal type. The general consensus from the program was to use the "Average Integrated Target Strength" which is the average time-integrated energy. Furthermore, an Echo Metrics Subcommittee [Ref. 9] was formed to find signal-processor dependent metrics for the measurement of target strength. Theoretically, the incident energy encountered by the object would be reflected or absorbed and eventually reradiated at some later time providing no energy was stored or lost in the object. Therefore, it would seem that the average of the integrated energy would be an independent metric for all types of signals providing the integration time is extended to include all the return signal. Some standardization of target strength is being investigated so that data from independent experiments can be compared and integrated.

III. DATA ACQUISITION SYSTEM

A. BACKGROUND AND CONCEPT

The experiments were conducted in a water tank located in Room 019 in Spanagel Hall at the Naval Postgraduate School. The tank was approximately 1.5 m wide, 8 m long, and 2 m deep and lined with anechoic rubber material. For the targets used, wall reflections were of the same magnitude as the target reflections. Usually, it was easier to use pulsed signals and time discriminate for the target reflection. However, the small dimensions of the tank did not provide the environment to do this effectively for all geometries. To overcome this difficulty, a subtraction technique was used employing a digital storage device. The basic concept was to subtract the signal received with the target immersed in the tank from the signal received with the target absent. The procedure was very simple and allowed for any target-source-receiver geometry.

B. DEVELOPMENT

A considerable amount of time went into the selection of the digital sampling and storage device, the source, and the receiver. The first question that had to be addressed was the range of frequencies to be used. The frequency range of 100-200 kHz was initially selected because it gave wavelength-to-target dimension ratios that match oceanic scenarios. The critical specifications for the digital storage device are the sampling rate, dynamic range and jitter. Dynamic range was not a problem since most digital oscilloscopes have the same voltage range as a typical non-digital oscilloscope. The sampling rate must be fast enough to provide a good representation of the signal, and assuming a sinusoidal signal about ten samples per

cycle would give a good trace. For example, for a 100 kHz signal the sampling rate would have to be 1 MHz. Another major concern was the amount of jitter in the sampling device. Jitter describes the fluctuation in the triggering times relative to the sampled signal. For a system using a subtraction process, it is perhaps the most critical specification because there has to exist a common time reference between collected waveforms to get accurate results.

The selection of the digital oscilloscope was based on the availability of equipment. Two digital oscilloscopes were evaluated. The Nicolet 3091 was analyzed first. Its fastest sampling rate was 1 MHz and had a storage capability of 4000 points. The Nicolet 3091 had a RS-232 serial interface and was easy to use, however it was not acceptable due to excessive jitter at the frequencies of interest. The jitter was easily seen by applying a pulsed signal and observing the traces on the scope. The digital oscilloscope finally used was the Tektronix 2430 (Tek 2430). It is a very capable osciiloscope and has many nice features making it suitable for data acquisition. The most important feature that it had was an averaging mode selectable from 2 to 256 waveforms. This helped eliminate random noise and minimized any fluctuations the electronic equipment possessed. The amount of jitter was dependent of the time scale selected. The fastest sampling rate of the Tek 2430 was 100 MHz which could be used to sample a 10 MHz signal using ten points per cycle. The jitter specification given in the operating manual, for the time-delayed mode, was .08 x (time scale). The jitter was observed and was significant for the time scale desired, however the saving factor was the time averaging mode which ultimately averaged out the jitter and provided a sufficiently constant time reference. It was very easy to observe this on the oscilloscope because of a triggering marker on the signal. Jitter becomes less of a problem for any digital

oscilloscope when the number of samples per cycle of signal increases. However, the problem then arises from the limited amount of storage in the oscilloscope. A smaller number of cycles can be stored when using a faster sampling rate. The Tex 2430 has a storage capabiltiy of 1024 points, much less that the Nicolet 3091; however it also has a time-delay feature which allowed for selective data storage (The Nicolet 3091 did not have any time-delay feature). Other features of the Tek 2430 include cursor control for voltage and time measurements, simple output to a Hewlett Packard Think-Jet printer or pen plotter, and a GPIB interface. It is a very versatile piece of equipment and was finally selected for use in the data acquisition system.

The selection of the source and receiving hydrophone was also limited to in-house equipment. For the frequencies desired, the USRD type F41 transducer was the appropriate choice with a nominal frequency range of 15-150 kHz [Ref. 10:p. 5]. It is a piston type piezeoelectric transducer with a face diameter of 10 cm. The choice of the receiver was a Celesco LC-10 hydrophone. It has a wide nominal frequency band, is small and light making it easy to move around, and has good sensitivity.

C. SYSTEM SET-UP

1. Electronic Equipment

The F41 source had to be driven near 200 V rms for target reflections to be seen. An Instruments, Inc. Model L2 power amplifier was used to drive the source and its selection was again based on what was available in the laboratory. It allowed for impedance matching and has a voltage-divided 10 mV/V port to monitor output voltage. The output of the receiver was passed through an Ithaco Model 1201 Low Noise preamplifier which has bandwidth setting capability. This was very

beneficial because there was a lot of 60 Hz noise which had to be eliminated by bandwidth filtering. The signal out of the preamplifier was sent to a Kikusui COS5060A oscilloscope and the Tektronix 2430 digital oscilloscope. Having a non-digital oscilloscope made observing and measurement of the waveforms easier to perform on the Tek 2430. A Hewlett Packard 3314A function generator was used to provide the source signal. It also provided the triggering signal which was sent to the external channels of the oscilloscopes. In the pulse mode, the HP 3314A sends out a 3 V transistor-transistor logic signal via its trigger port. The pulse repetition rate of 10 ms was sufficient to allow reflections to diminish before the next pulse. A Hewlett Packard 9000 Series 300 desk top computer was used as the data collection and processing unit. It was connected to the Tek 2430 via the HPIB bus. The transfer of waveforms stored on the Tek 2430 was controlled by software programs. Data was ASCII encoded from the Tek 2430, transferred, decoded into actual voltages, and then stored onto disks in binary data form. A schematic diagram of the electronic system is shown in Figure 4.

2. Physical Set-up

To measure all possible bistatic angles, the scattering pattern would have to obtained in three dimensions. This was not done in this work. Bistatic data were limited to the horizontal plane determined by the source, receiver, and target, with the axis of the target in the same plane.

The source, the F41 transducer, was mounted on a 3/4-inch aluminum rod attached to a rectangular support plate. The rod was fixed to the plate by means of a friction fitting secured by a hose clamp. Target, source, and receiver were submerged one meter below the surface of the water and the rods which supported them were marked for this depth. The source with its support rested on another

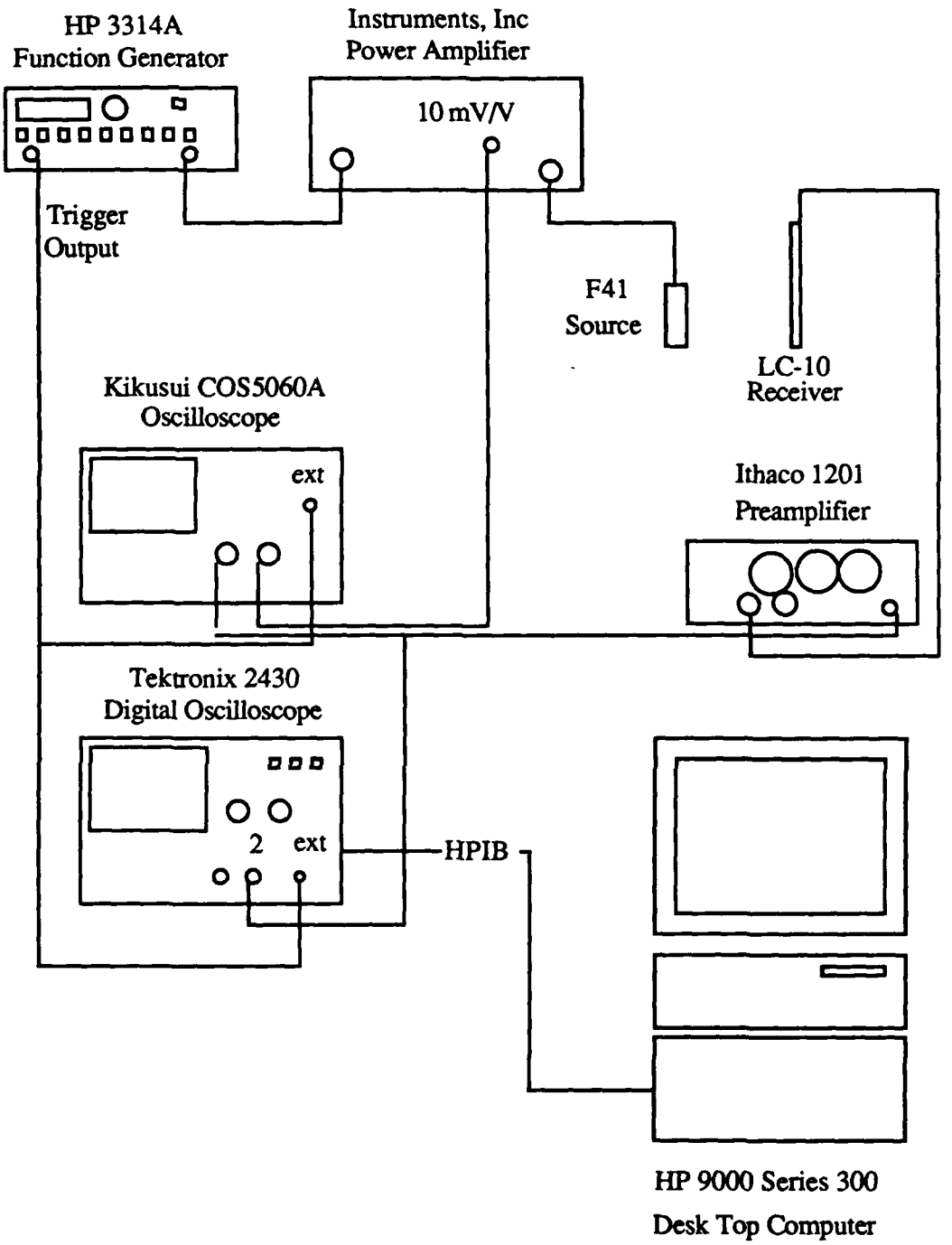

Figure 4. Data Acquisition System

support built from aluminum L-beams that spanned the width of the tank. Lead bricks were used to hold the source once it was set in place and a level was used to ensure the source face was vertical. The receiver was mounted onto a sliding track specially built for the tanks. Adjusting screws were added for ease of positioning the receiver vertically. The initial intent was to design a rotating boom to hold the receiver and support the target from its center. A device was constructed, but too much receiver movement occurred between the loading and unloading of targets. Though the boom was never used, the device was still used for the suspension of targets and had a mechanical angle indicator on its top for angle measurement. Spherical targets were suspended by a thin cable and the cylindrical target by a 3/8-inch rod.

The direction of the source was set by aligning the source, receiver, and target along a straight line with the receiver between the source and target. Source, receiver, and target depth were one meter. Vertical alignment was ensured by keeping the source and receiver vertical by use of a level. The frequency was set to 200 kHz to establish a narrow major beam and the source was rotated until maximum signal was seen by the receiver. This ensured the target was being totally ensonified by the major lobe of the source.

Once the source direction was set, the receiver was moved to the desired position. The angle between the source, target, and receiver was determined by setting the receiver's track perpendicular to the source-target axis and then using trigonometry relationships. After the desired geometry was set, care was taken to ensure the target, source, and receiver were stationary. It was critical that all elements be stationary when waveforms were collected.

3. Data Collection

The method of data collection and storage followed the sequence:

- set up desired source-receiver-target geometry
- warmup all electronic equipment >1 hr
- ensure connections as illustrated in Figure 5
- load "Tex" onto computer
- set up the Textronix 2430 oscilloscope
  - B trigger mode to "runs after"
  - A trigger
    - mode: normal
    - coupling: AC
    - source: external 1
    - slope: positive
    - level: 800 mV
    - trigger position: 1/8
  - data encoding: ASCII
  - GPIB address: 4
  - vertical mode: channel 2
  - select time delay to obtain desired time window
  - set acquisition mode to 256 averaging
- adjust channel 2 voltage scale/Ithaco gain appropriately for the signal
- for each new signal, press the acquire button
- wait sufficient time for averaging to take place
- press the save button
- run the "Tex" program

The "Tex" program controlled the transfer and storage of data from the digital oscilloscope. Inputs from the user were file names and file descriptions. The transfer process, including writing onto the disk, took approximately 10 s per waveform. A listing of the program is in Appendix A.

The computer program "Plot" was used to evaluate the stored data. It took two files and subtracted them, and then plotted the results on the CRT terminal. Hard copy output could be obtained by porting to a pen plotter or Think-Jet printer. Input from the user required file names and where printout was to occur. The plotting routine was written so that the plot's parameters were easily changeable. A listing is enclosed in Appendix B.

The method of data collection was a slow and somewhat tedious process since all movement of target and receiver ware manually controlled. Data readings were also recorded manually.

4. Validation

The question of whether the data acquisition system could correctly extract a target reflection immersed within other signals had to be answered. The very simple procedure of subtracting background noise works only if there is a common time reference for "target in" and "target out" waveforms. For ease of discussion, "background noise" is used for any signal, random or coherent, that is not the desired signal and corresponds to the "target out" condition.

The procedure to validate the system began with obtaining a geometry which allowed a direct pulse and reflected pulse to be completely separated by time discrimation with no interfering wall reflections. *Figure 5 is such an example.* The larger pulse was the direct path pulse and the second pulse is the pulse reflected from a styrofoam sphere. The frequency was 66.5 kHz and the pulse length was 20 cycles. The reflected pulse is shown enlarged in Figure 6. The peak-to-peak voltage of the reflected pulse was measured to be 68 $\pm$ 2 mV using the cursor controls of the Tek 2430.

The pulse length was then increased to 120 cycles so the direct pulse would be interfering with the reflected pulse. No other changes were made. The interference of the two signals is shown in Figure 7 and was stored in file A. Next, the sphere was removed and the background noise sampled and recorded in file B. The background noise in this case was mostly the direct pulse. The last step was to subtract file B from file A to get the reflected signal from the sphere. The result is shown in figure 8. The waveform begins at the same time in comparison with Figure 6 and the only difference is that the pulse length was longer as expected and the curve slightly more choppy in form. Measured voltage was 73 ± 4 mV. The larger uncertainty arose due to the combination of small jitter and amplitude fluctuations of the HP 3314A. The uncertainty was estimated beforehand by taking identical signals directly from the function generator to the Tek 2430, recording them in separate files, and subtracting them and observing the results. It was found that peak-to-peak voltage uncertainty was approximately four digitizing levels regardless of the voltage scale used (a digitizing level equals the voltage per division divided by 50 for the Tek 2430). Given that this error would always be present, there was good agreement between Figure 6 and Figure 8, and the method of obtaining data was considered validated.

As with any signal processing system, a high signal-to-noise ratio is desired. For any digital subtraction routine, the desired signal has to be large enough relative to the noise so it will not disappear in the digitizing level of the sampling device. For example, if noise plus the signal were 10 volts using 512 digitizing levels or bins, each bin represents 19.5 mV. If the signal were small, i.e., 1 mV, the signal level would be much smaller that the digitizing level and would be lost in the subtraction routine.

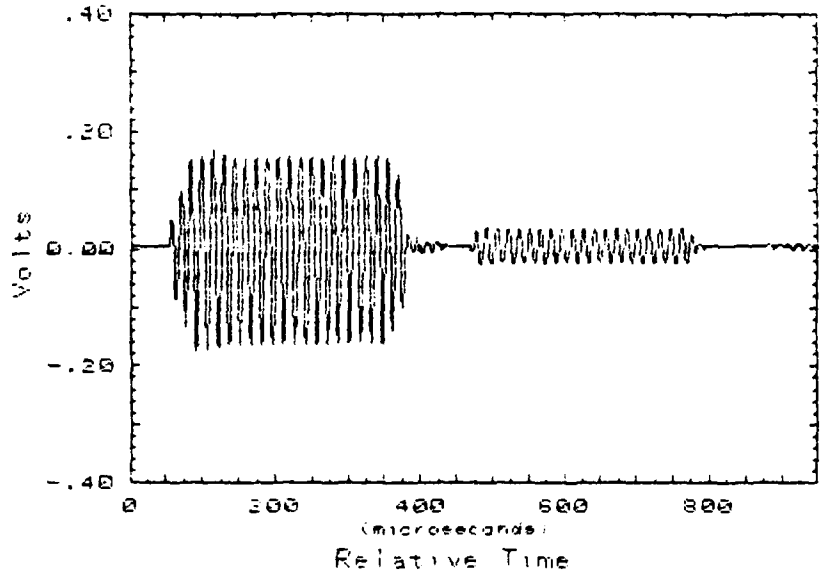

Figure 5. Direct and Reflected Pulse

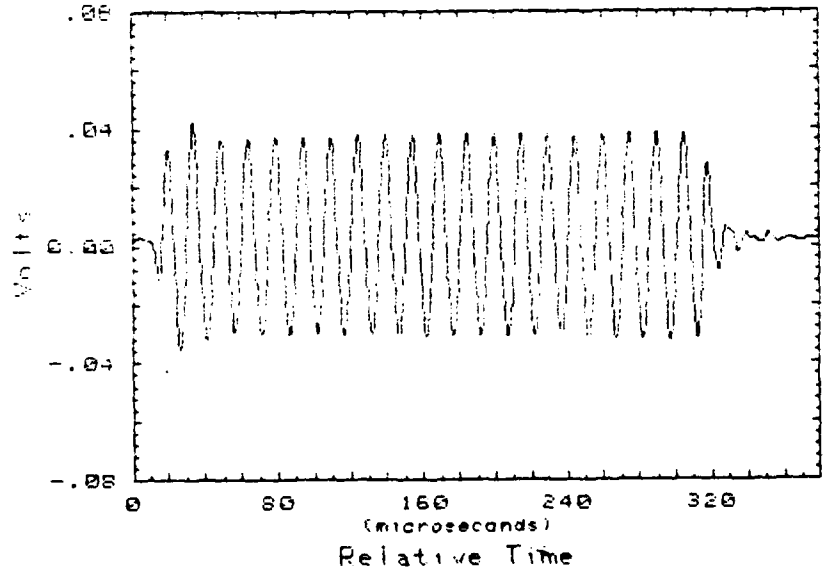

Figure 6. Reflected Pulse

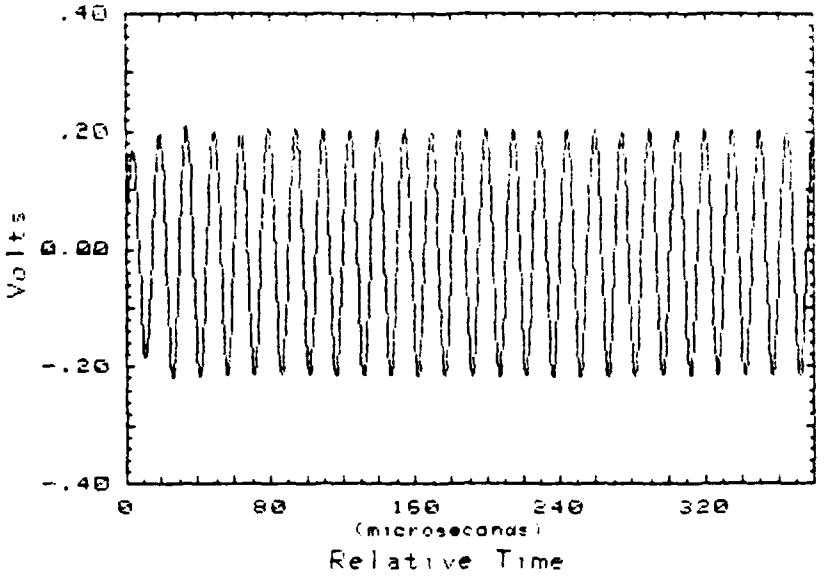

Figure 7. Interference Between Direct and Reflected Pulse

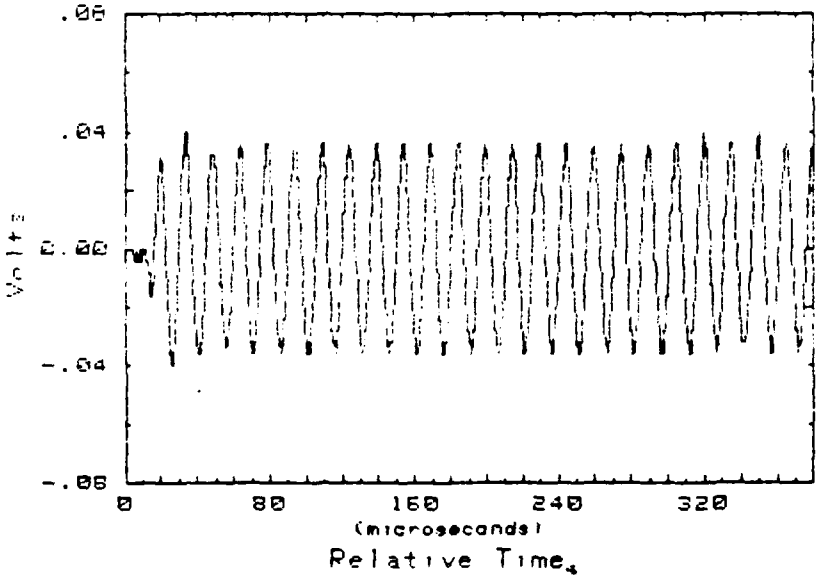

Figure 8. Reflected Pulse, N=120

Keeping the source and receiver positions fixed relative to each other was critical. Small movement between the two greatly affected the phase of the received signal and had a large effect on the results. This effect was verified in preliminary work. The initial intent was to place the receiver and support the target on the same platform. However, the removal of the target for the background noise measurement caused flexing in the platform and produced source-to-receiver movement giving incorrect results in the subtraction routine. Figure 9 illustrates the effect of source-receiver movement on "target-in" and "target-out" waveforms. The solid trace represents the target-in waveform and the dashed line represented the target-out waveform. The reflection began at 35 usec. The dashed and dotted line is the the result from the subtraction of the two waveforms and it was clear that in this case, it did not give the correct results. The region between 0 and 35 usec should have cancelled to zero. The non-zero result indicates a phase change caused by relative source-receiver movement. The phase change subsequently affected the amplitude of the reflected signal from 35 to 100 usec. It was easy to see that any phase change brought about by small source-receiver movement would cause erroneous results. To eliminate this problem, a separate platform was subsequently built and used for the receiver.

The output of the power amplifier was also checked in preliminary work for fluctuations. An arbitrary source-receiver geometry was selected without any target in the tank. Several waveforms of the direct pulse were stored at various times after initial start up. Amplitude fluctuations existed shorty after start-up. Ideally, successive waveforms subtracted from each other would cancel out to give a zero response. If amplitude fluctuations existed a false signal would occur and this in fact did occur after five minutes of warm-up as Figure 10 illustrates. Another

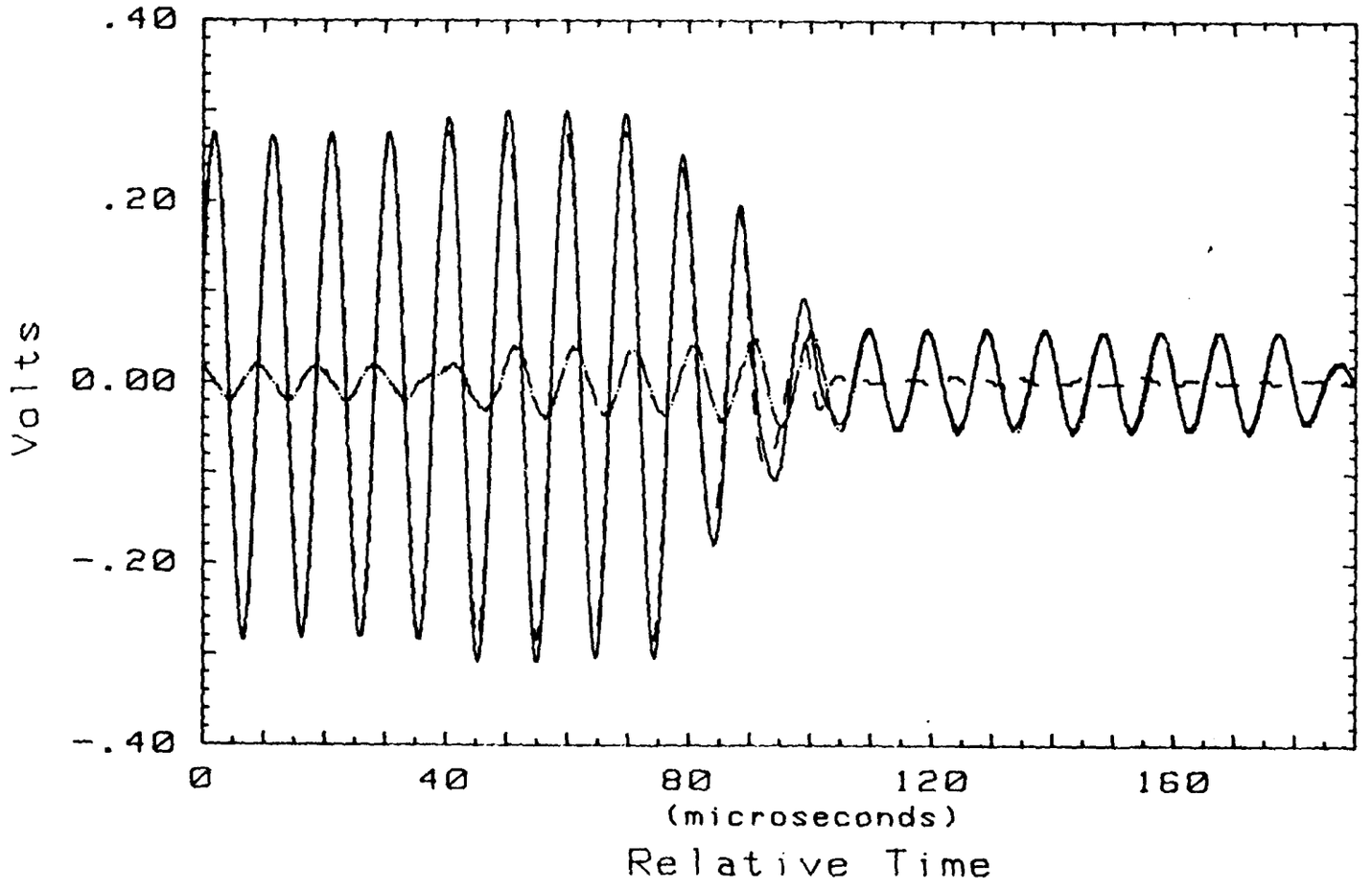

Figure 9. Relative Source-Receiver Movement Effect

test taken at 15 minutes after start up produced better but still unsatisfactory results. After one hour of warm-up the amplitude fluctuations subsided and a zero respose was obtained.

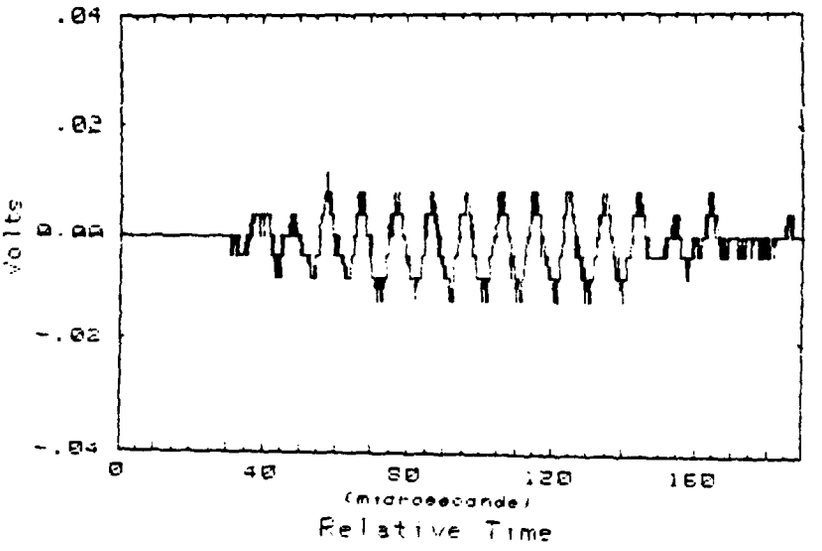

Figure 10. Waveform Amplitude Fluctuation Effect After 10 Minutes of Warm-up

IV. FAR FIELD DETERMINATION

The measurement of the far field of several objects was conducted. An equation that gives the approximate beginning of the far field is given by [Ref. 2:p. 188]:

$$r_f \approx \frac{L^2}{4\lambda} \qquad (3)$$

L = the longest dimension of object
λ = wavelength

It is always best to determine the far field by measuring pressure amplitude as a function of distance from the object. The equation for a diverging spherical wave, as described by equation 2, can be manipulated by taking the log of both sides to transform it into a linear equation with a slope of minus one. The far field can be determined experimentally when the observed slope of the curve starts to deviate from minus one.

The far field of the F41 was determined to begin at approximately 100 cm and 70 cm for 176 kHz and 70 kHz, respectively. The far field for the sound reflected from the styrofoam cylinder positioned broadside to the source was determined to begin at 40 cm for 70 kHz. The three-inch diameter styrofoam sphere's far field began at less than 20 cm at 70 kHz. Figures 11 through 14 are graphs of the data used to determine their far fields. Lines of slope equal to minus one are drawn on the graphs.

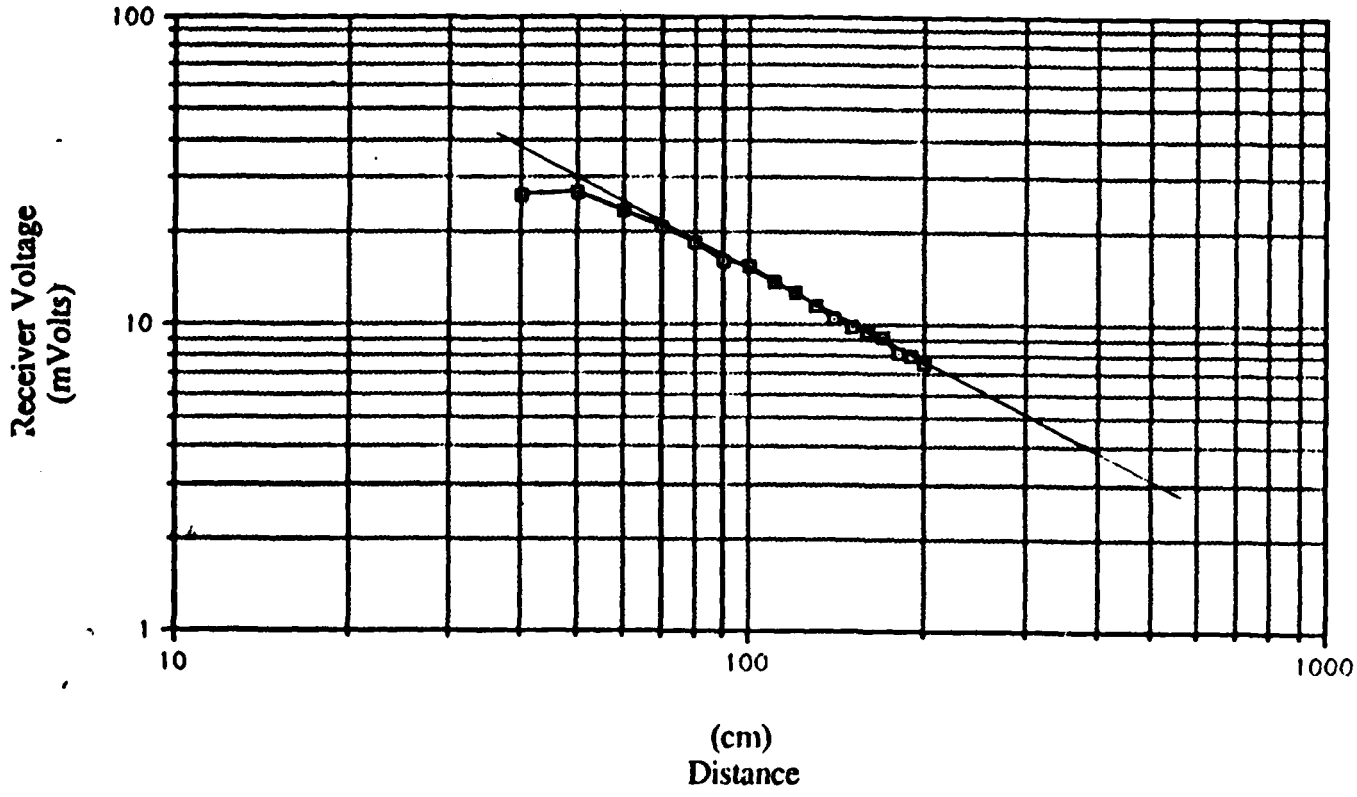

Figure 11. Receiver Voltage vs Distance, F41, 176 kHz

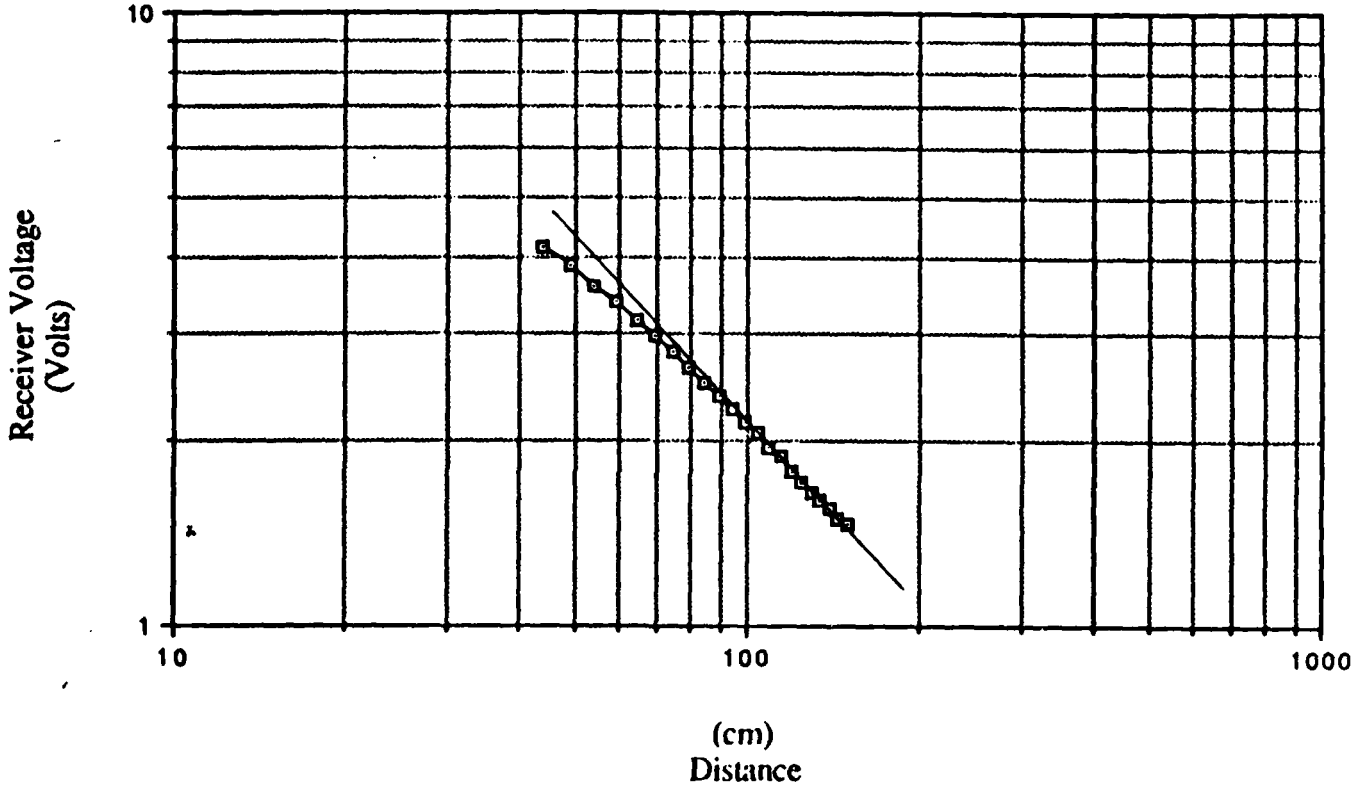

Figure 12. Receiver Voltage vs Distance, F41, 70 kHz

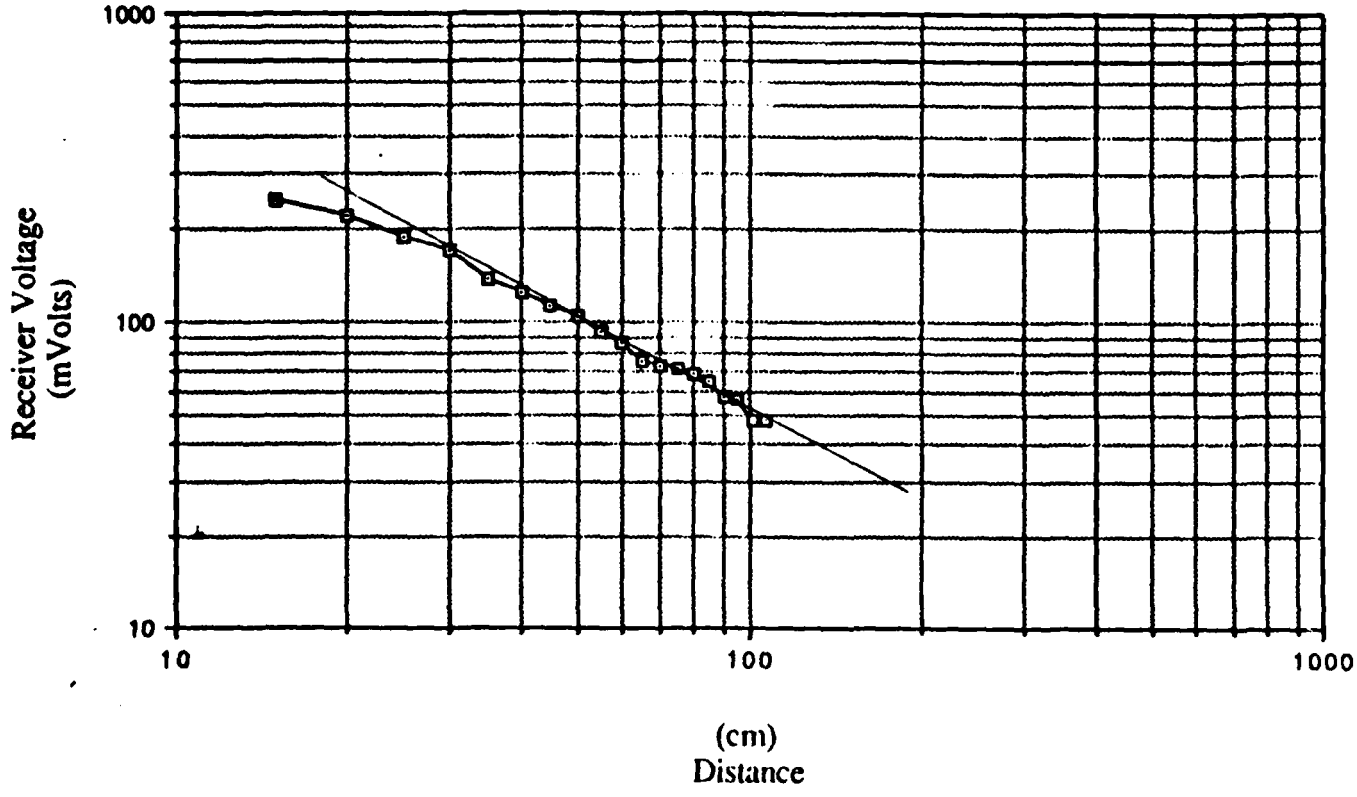

Figure 13. Receiver Voltage vs Distance, Cylinder, 70 kHz

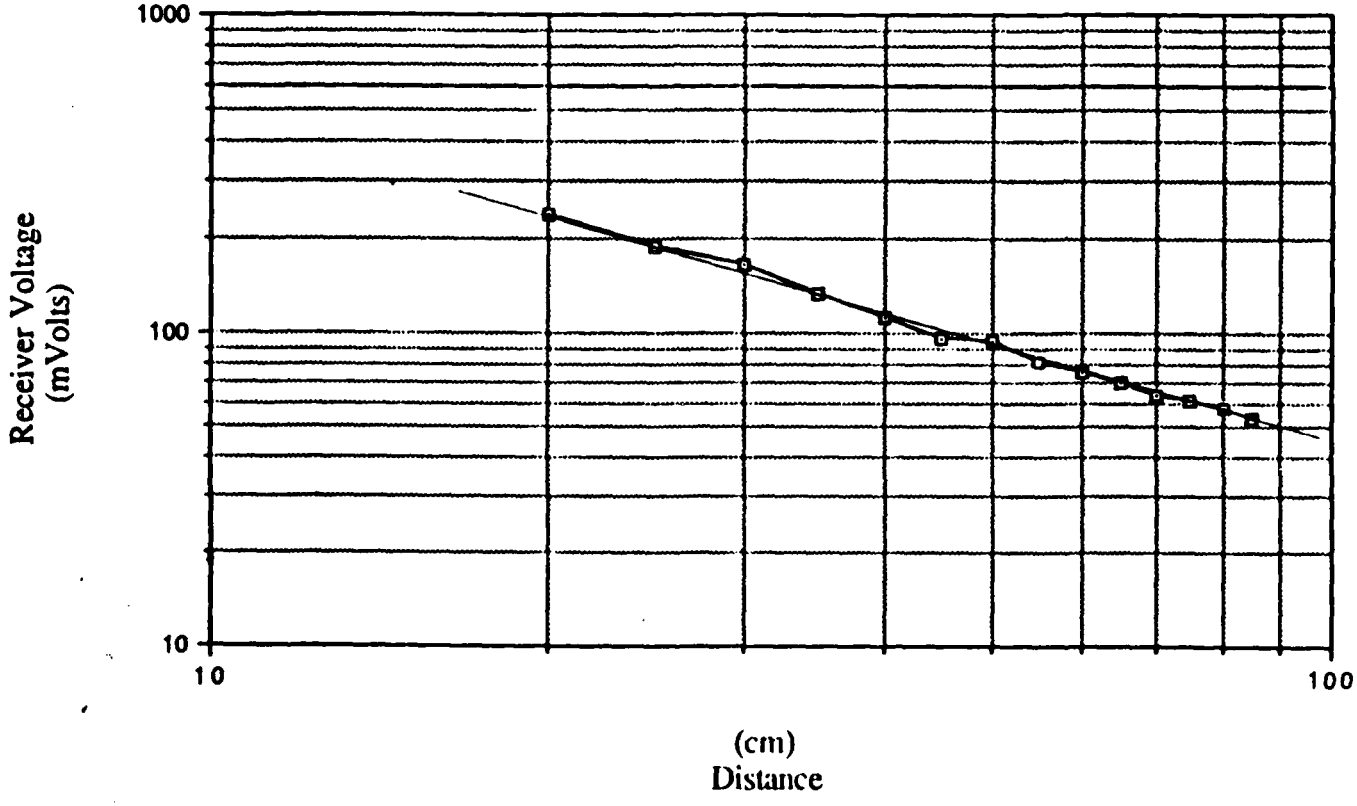

Figure 14. Receiver Voltage vs Distance, 3-Inch Diameter Sphere, 70 kHz

V. SPHERES

A. INTRODUCTION

To achieve an understanding of the complexities involved in analyzing scattering effects of various objects, it was instructive to begin with a very simple and symmetrical object, a sphere. Several solid metal spheres were used. Spheres were aluminum and brass, but, the exact composition was not known or investigated since they were to serve only as preliminary tools in studying the general properties of waveform scattering.

Since metal spheres are not perfectly rigid, they are capable of absorbing energy and subsequently reradiating it. Also, they possessed resonances. Many experiments in the past 30 years have been conducted with spheres and long cylinders, and the Resonance Scattering Theorem (RST) has evolved from this work [Ref. 5,6,7,8,11,12,13,14]. This theorem predicts scattering patterns which entail both the rigid-like properties and the resonance properties of an object. It was not the intent to examine this theorem in detail but only to observe some of its predictions experimentally.

B. MONOSTATIC FORM FUNCTION

The goal of replicating some of the data in the literature was sought to establish confidence in the experimentation process. Neubauer, Vogt, and Dragonette [Ref. 7] conducted an analysis on elastic spheres using steady-state signals and observed the backscattered signal form function from an aluminum sphere as a function of ka. The reflection form function is defined as:

$$f = \frac{2r}{a}\left|\frac{p_s}{p_o}\right| \qquad (4)$$

p_s = scattered pressure amplitude measured at r
p_o = incident pressure amplitude at sphere center
a = sphere radius

Their experimental data were plotted and compared against theoretical results and good agreement occurred.

Part of Neubauer's experiment was repeated. A four-inch diameter aluminum sphere was ensonified by 50 cycle pulses from 100 to 130 kHz, and the backscattered pressure amplitude was measured. Time discrimination of the reflection was used. The amplitude of the reflected pulse was taken at what was judged to be the steady-state part of the signal. The receiver was 1.60 m from the center of the sphere, placing the receiver well within the far field of the sphere.

The wavelength used in the calcuation of ka was dependent on the speed of sound in the water, which in turn was affected by temperature, pressure, and salinity. For the fresh water tanks, salinity was ignored. The speed of sound was based on an empirical formula that applied to distilled water [Ref. 1:p. 107]. Although the water was normal tap water, the distilled water formula was a close enough approximation [Ref. 15]. Water temperature of the tank was a consistent 17 degrees Celsius throughout the entire experimentation phase. At this temperature and normal atmospheric pressure, the speed of sound was calculated to be 1473 m/s. Experimentally, two LC-10's were placed on a track 180 cm apart and the successive arrival times of the pulse were measured via the Tek 2430 with the cursor controls. The speed of sound thus was measured to be 1480 ± 20 m/s, placing 1473 m/s well within the experimental uncertainty, and this value was used as the speed of sound in water.

The shadowing effect of the LC-10 in front of the F41 source was taken into account by placing a dummy LC-10 at that position and recording incident pressure at the sphere center location. Additionally, since the LC-10 was not perfectly omnidirectional, the support rod was marked to maintain a constant receiver aspect with the target. Placing the LC-10 in front of the F41 also caused additional reflections to occur. The direct pulse was reflected by the LC-10 back to the source's face and again reflected there back to the LC-10. More "noise" was present when measuring the monostatic case but appropriate location of the receiver eliminated any interference from those reflections.

The data matched Neubauer's results well, and the form function as a function of ka is plotted in Figure 15. Data from Neubauer's experiment is also plotted in Figure 15. The only difference between results was a small shift in ka of approximately 0.2-0.3, not surprising since the compostion of the sphere was unknown. The minima corresponds to resonant frequencies of the sphere, where the specularly reflected wave is interfering with the resonantly radiated wave from within the body.

C. WAVEFORM EFFECTS

The effect of a sphere's resonance was examined in more detail. A four-inch diamter aluminum sphere was ensonified by a 30 cycle pulse at, above, and below a resonant frequency of 82.7 kHz. At resonance, the ringing of the sphere is clearly seen in Figure 16 when the direct pulse ends. Pulse length was approximately 367 μs long. The sphere's stored energy is simply being reradiated. Figures 17 and 18 show the waveform response 2 kHz above and below resonance. They are decisively different and clearly illustrate the resonance effect.

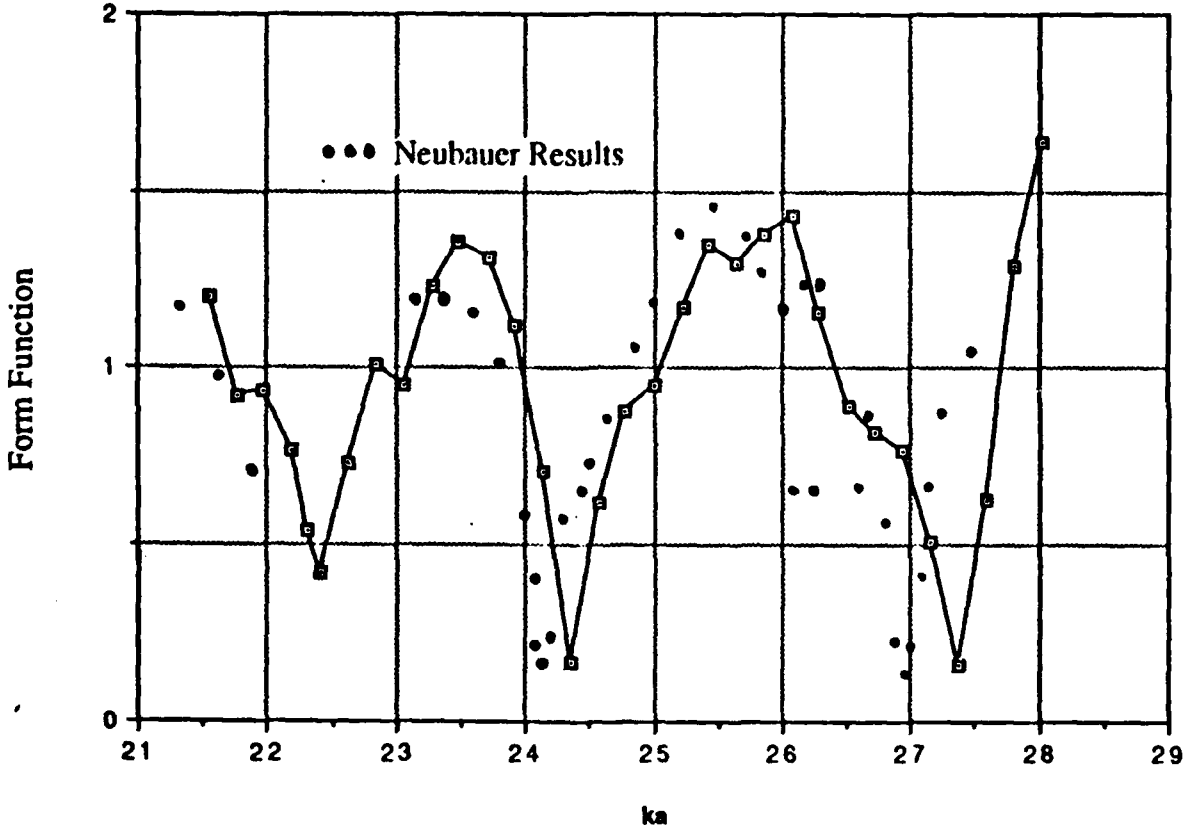

Figure 15. Backscattered Form Function vs ka, Aluminum Sphere

The effect of sphere composition on reflected waveforms was observed. A four-inch diameter brass sphere was ensonified by the same frequencies as the aluminum sphere. Brass has a characteristic impedance approximately 2.5 times that of aluminum. Figures 19, 20, and 21 show the reflected waveforms having frequency dependence that are markedly different from the aluminum sphere.

The effect of pulse length was observed using a 4-inch aluminum sphere at and off a resonant frequency. Figure 22, at resonance, and Figure 23, off resonance, show reflected wavforms using a short pulse of 2 cycles. They appear very similar in shape. Figures 24 and 25 show the results for a pulse length of 5 cycles. Again, the results of the two are similar. When pulse length reaches 15 cycles, the effects of the resonance begins to be clearly observed, as Figure 26 and 27 illustrate.

For comparison, the same procedure above was performed on a four-inch diameter brass sphere. Results are illustrated in Figures 28 through 33. The brass sphere did not show any resonance effect as determined in the preceding composition experiment for these frequencies, so its results were very similar to the aluminum sphere's results off resonance. Waveforms were practically identical for the shorter pulse lengths regardless of frequency and composition implying the reflections are purely specular. The results clearly demonstrated the dependence of pulse length on reflected waveforms.

D. SELECTION OF STYROFOAM

Since defining target strength becomes difficult when using elastic spheres, which was not the intent of this work, the need existed to do one of two things: (1) work at a frequency that gives good replication of the input pulse, or (2) find a target that gave a very high impedance mismatch.

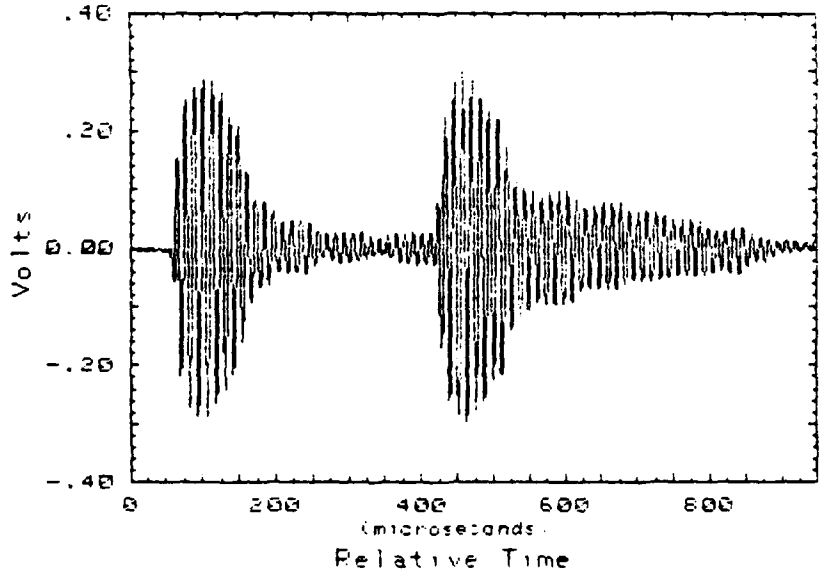

Figure 16. Aluminum Sphere Reflection at Resonance, 82.7 kHz

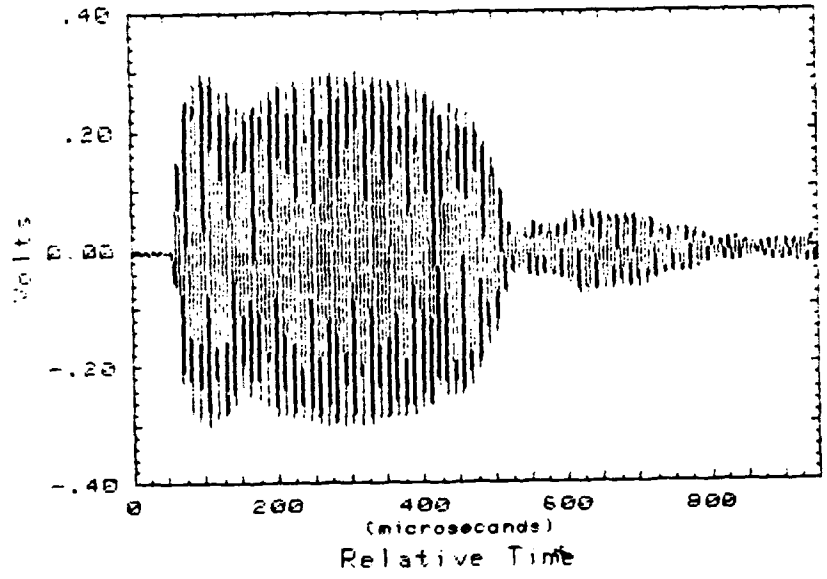

Figure 17. Aluminum Sphere Reflection, 84.7 kHz

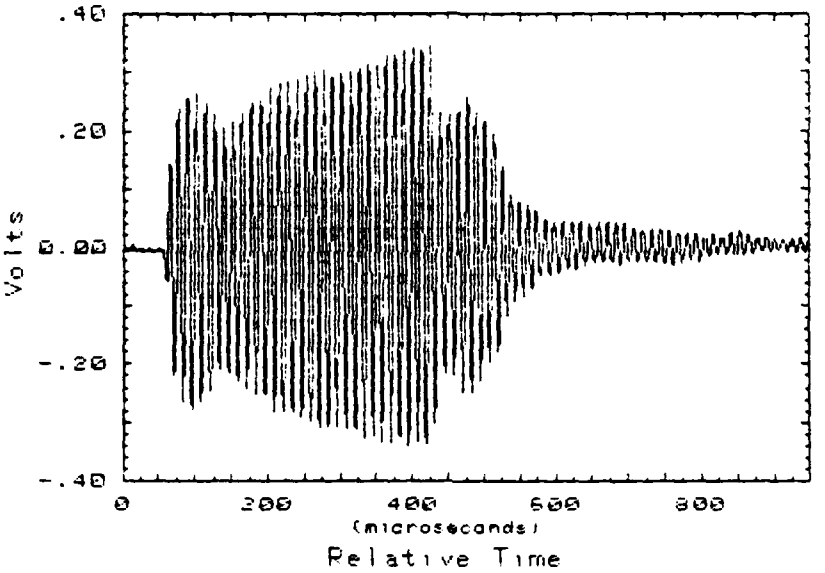

Figure 18. Aluminum Sphere Reflection, 80.7 kHz

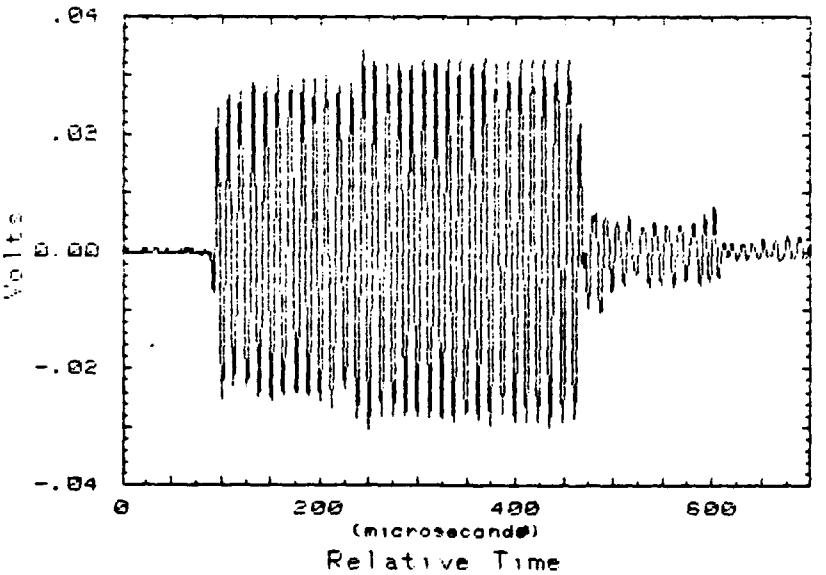

Figure 19. Brass Sphere Reflection, 80.7 kHz

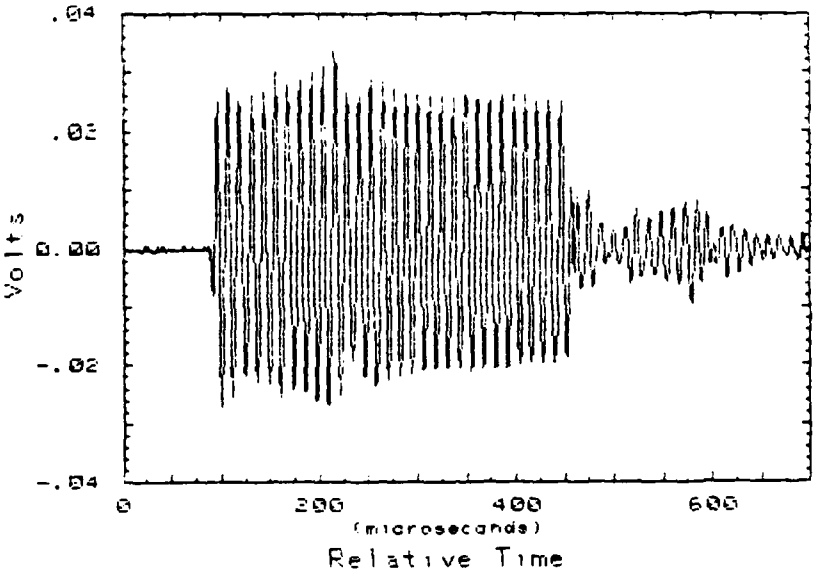

Figure 20. Brass Sphere Reflection, 82.7 kHz

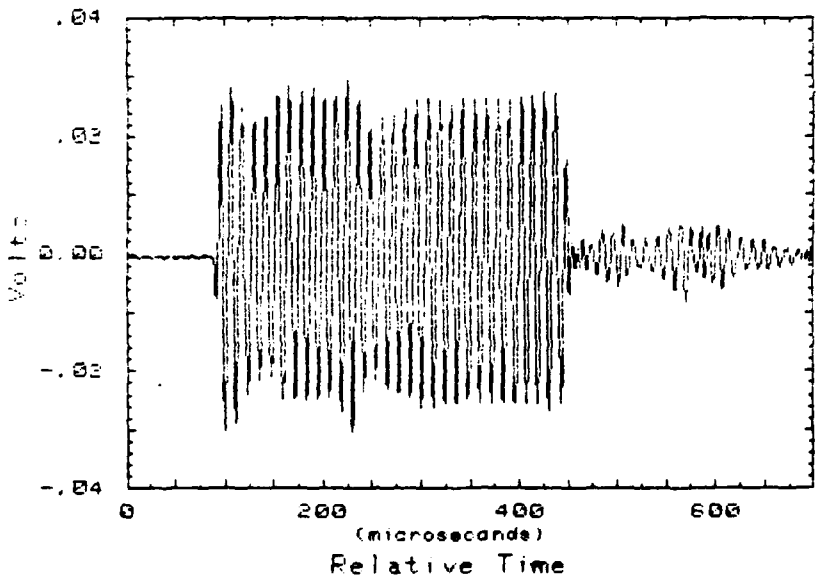

Figure 21. Brass Sphere Reflection, 84.7 kHz

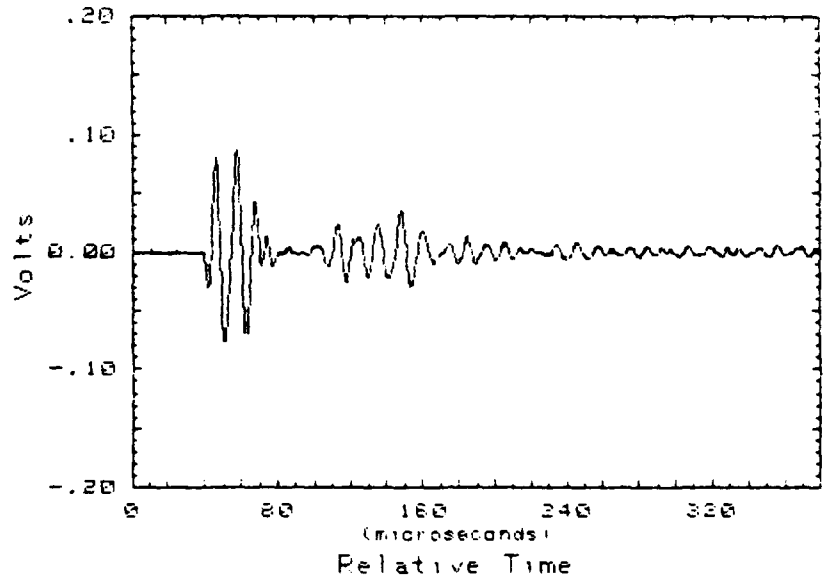

Figure 22. Aluminum Sphere Reflection, 82.7 kHz N=2

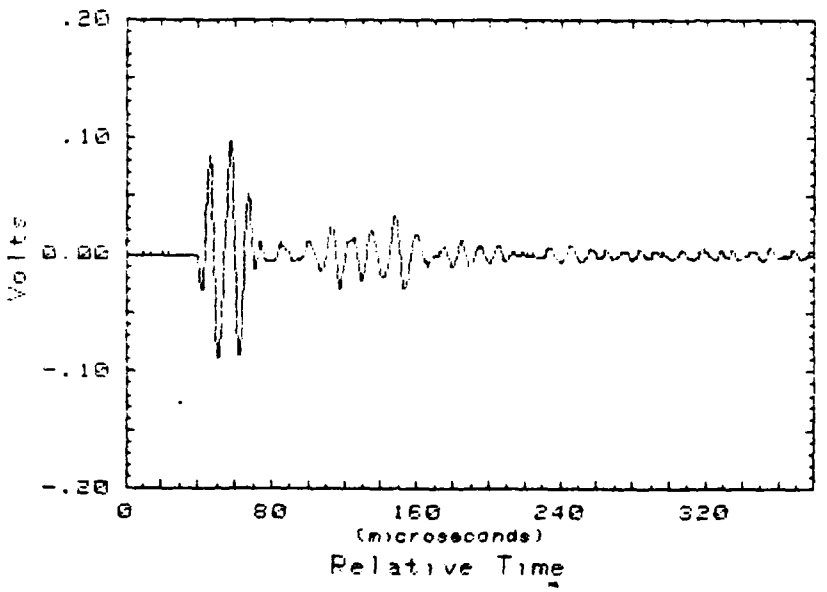

Figure 23. Aluminum Sphere Reflection, 84.7 kHz N=2

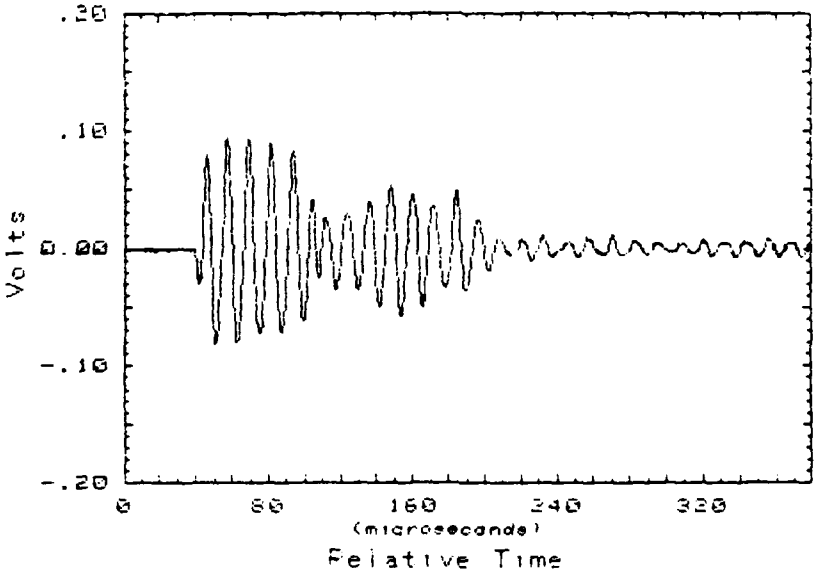

Figure 24. Aluminum Sphere Reflection, 82.7 kHz N=5

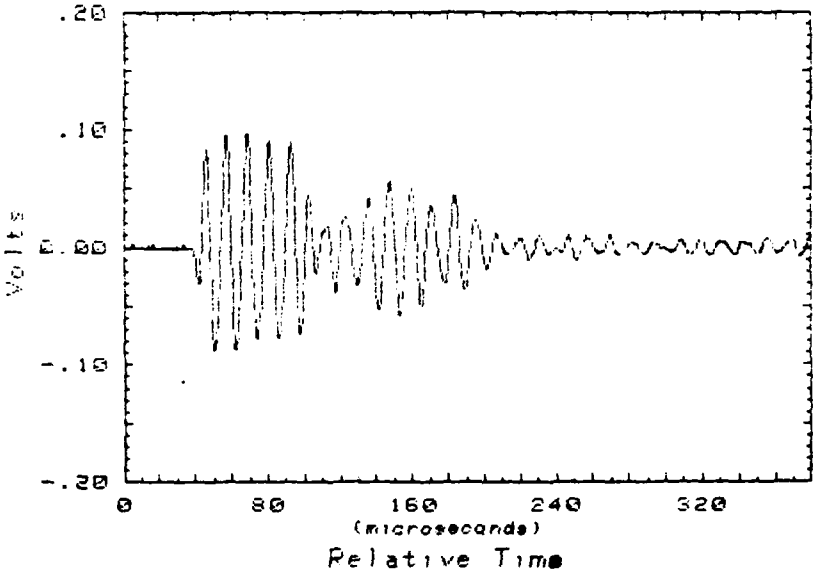

Figure 25. Aluminum Sphere Reflection, 84.7 kHz N=5

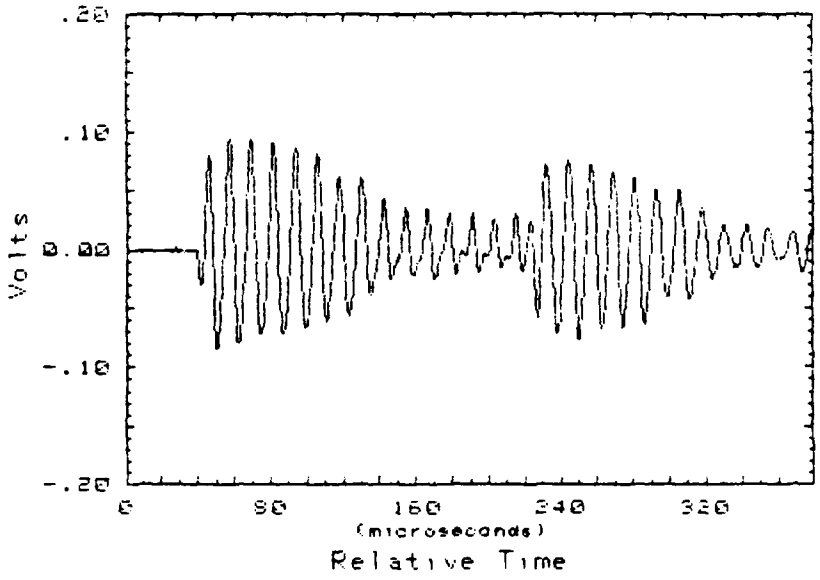

Figure 26. Aluminum Sphere Reflection, 82.7 kHz N=15

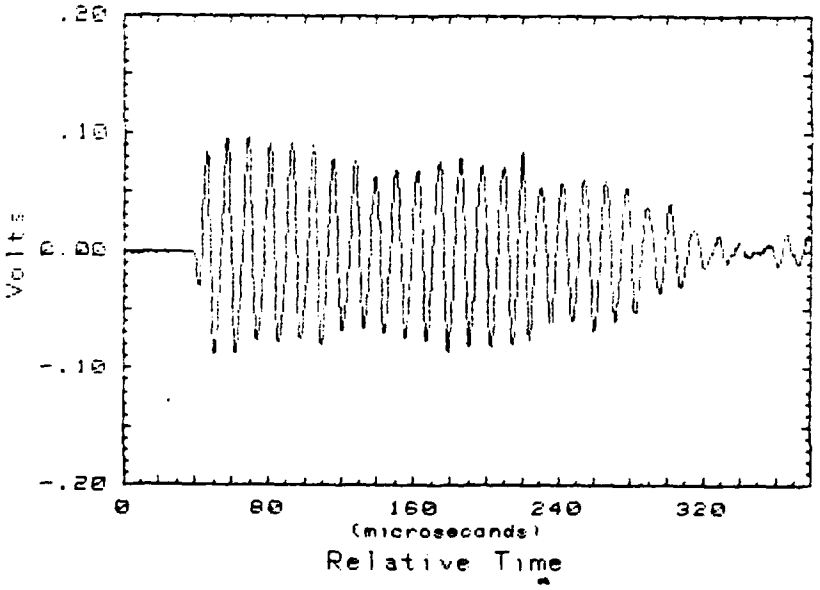

Figure 27. Aluminum Sphere Reflection, 84.7 kHz N=15

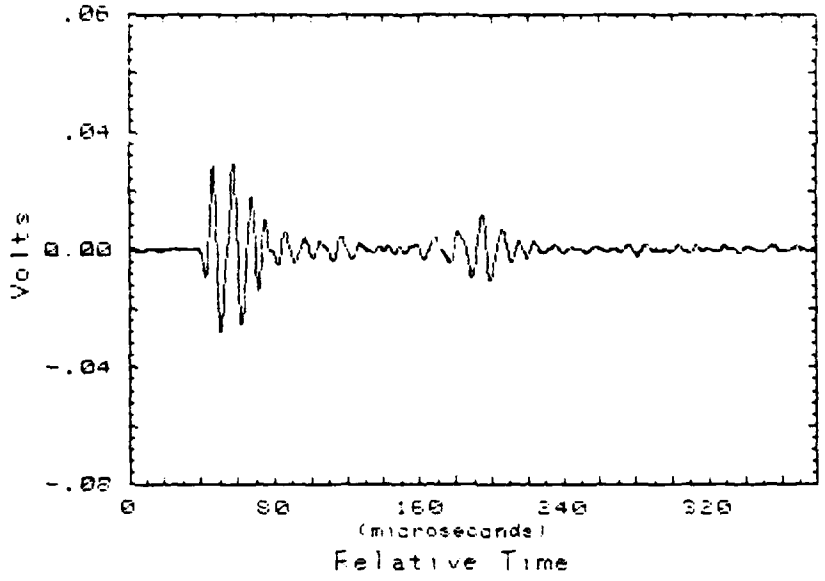

Figure 28. Brass Sphere Reflection, 82.7 kHz N=2

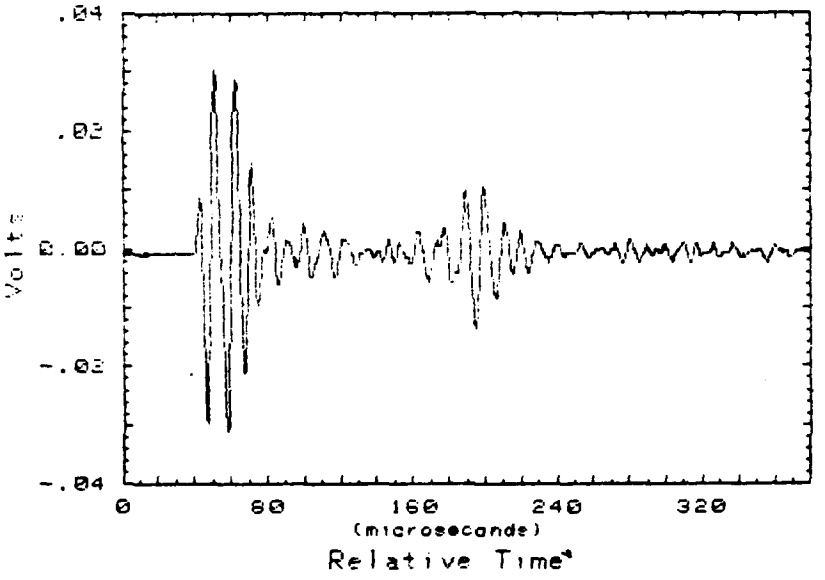

Figure 29. Brass Sphere Reflection, 84.7 kHz N=2

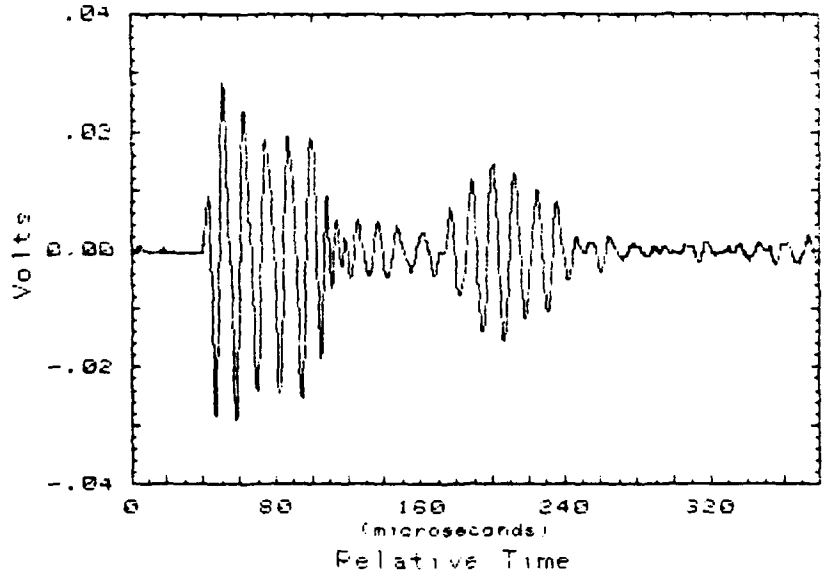

Figure 30. Brass Sphere Reflection, 82.7 kHz N=5

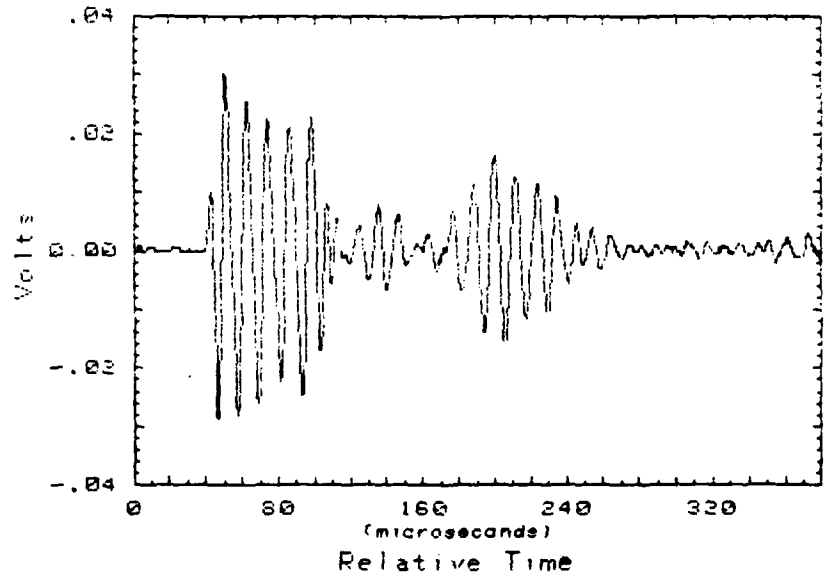

Figure 31. Brass Sphere Reflection, 84.7 kHz N=5

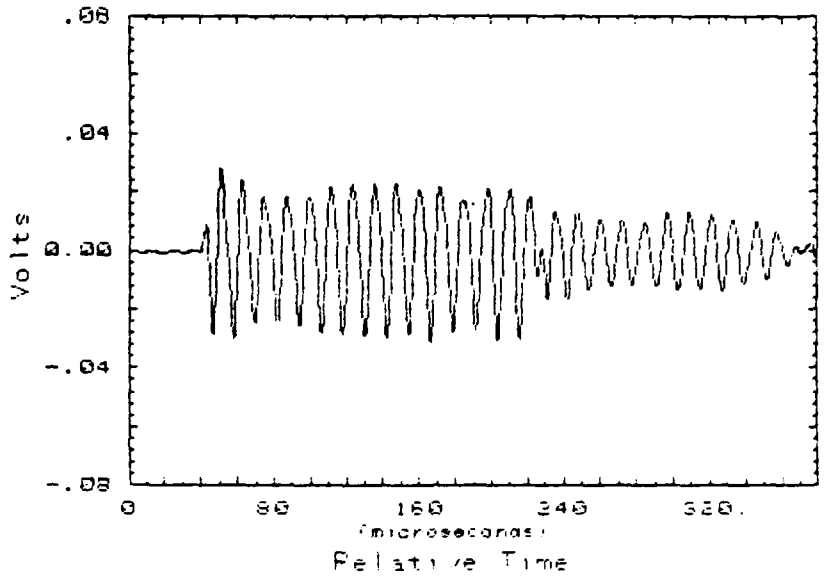

Figure 32. Brass Sphere Reflection, 82.7 kHz N=15

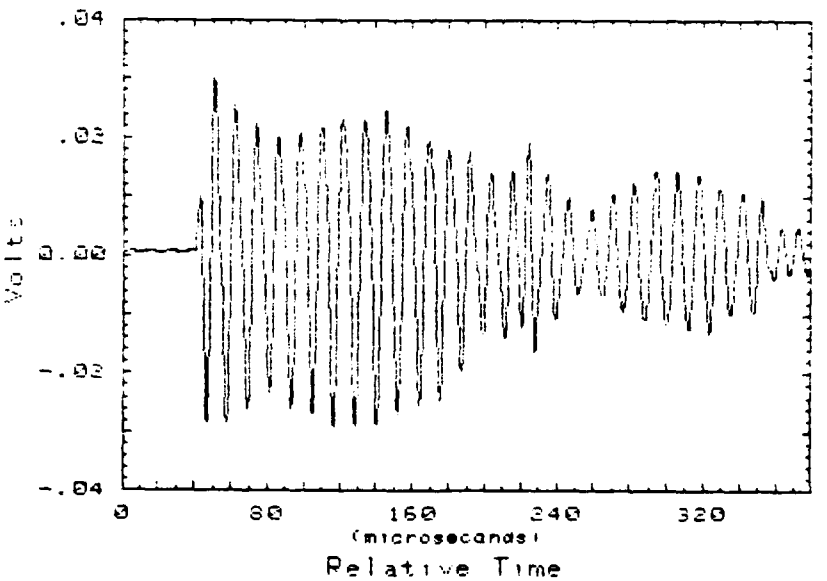

Figure 33. Brass Sphere Reflection, 84.7 kHz N=15

The most important factor in achieving a good reflection is the impedance mismatch between the fluid and object. Experimental work done with metal spheres by Hamptom [Ref. 5] shows the effect of compostion using several metals. A pressure wave in water will see little resistance to a hard rubber sphere because its characteristic impedance is near that of the water. An object that gives a high impedance mismatch is an air bubble. The impedance ratio of water to air is roughly 3000. For the case of an air bubble, the boundary condition between the water and air is termed "pressure release", since the pressure transmitted into the air is nearly zero [Ref. 2:p. 127]. The difference between a pressure-release sphere and a rigid sphere is best seen graphically in Figure 34 [adapted from Ref. 15: p. 359]. In the ka region used in the experiments, both the rigid and pressure-release form functions will be nearly identical and equal to one.

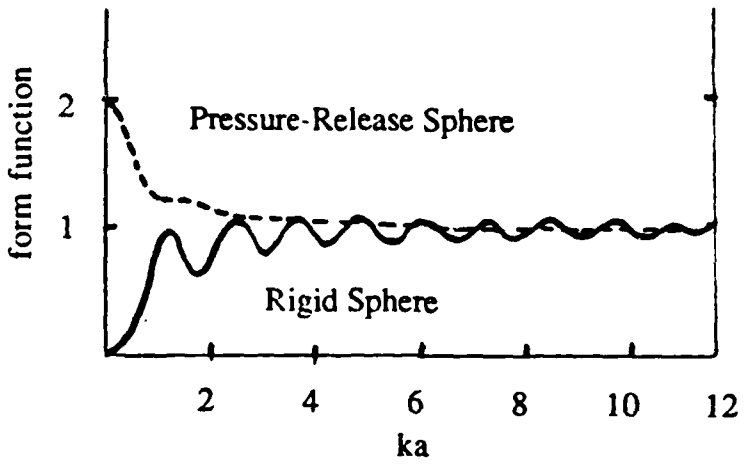

Figure 34. Backscattered Form Function of a Rigid and Pressure Release Sphere

A styrofoam ball was used to approximate an air bubble not near resonance. The reflected waveforms were generally identical to the input pulse at all

frequencies. This made styrofoam an ideal target for this work. Figures 35 through 40 show reflections from a three-inch diameter styrofoam sphere using various pulse lengths at 100 and 106 kHz.

E. BISTATIC SCATTERING

A 360 degree pattern of the pressure amplitude scattered from a styrofoam sphere was obtained to compare the results with theoretical predictions for a perfectly reflecting sphere. Since a sphere is perfectly symmetrical, it was not necessary to take the entire 360 degrees of data but only 180 degrees of it.

Theoretical equations have been derived and published by several authors that predict scattering of acoustic plane waves from a sphere [Ref. 16,17]. They tend to be quite complicated functions involving sums of Hankel functions. Figure 41 was adapted from Medwin and Clay [Ref. 16:pp. 192-193] and shows computed scattering patterns in relative amplitude for a perfectly reflecting sphere in water for several ka values. The incident plane wave is arriving from the right. The patterns show that for increasing ka the major forward lobe gets larger in amplitude and narrower in width. More structure, i.e., secondary lobes, develop as ka increases.

Bistatic data were obtained for a ka =10 using a three-inch diameter styrofoam sphere and are shown in Figure 42. The incident wave arrives from the bottom. Frequency was 61.5 kHz and an eight cycle pulse was used. The graphed data revealed some structure in the forward scattering region and a large forward scattering lobe. Comparison with the theoretical prediction for a rigid sphere (dashed line in Figure 42) show that the salient features of the scattered pattern were duplicated.

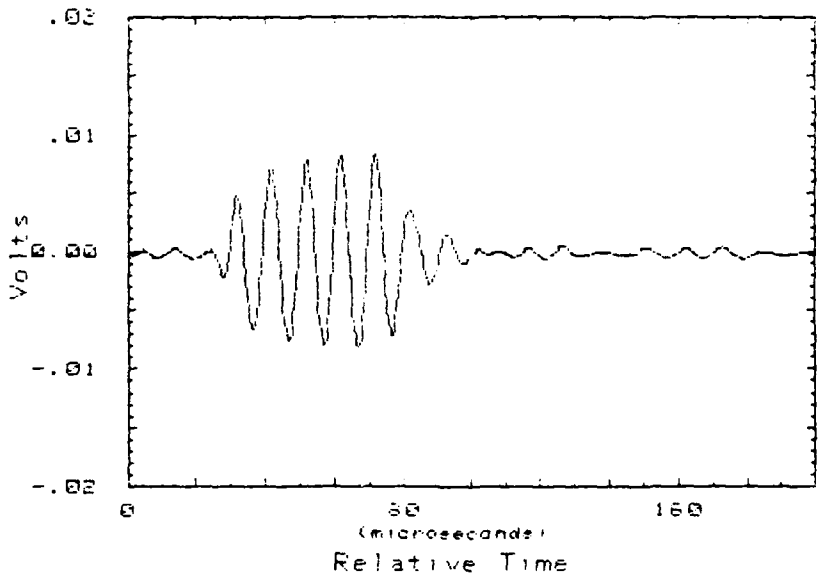

Figure 35. Styrofoam Sphere Reflection, 100 kHz N=5

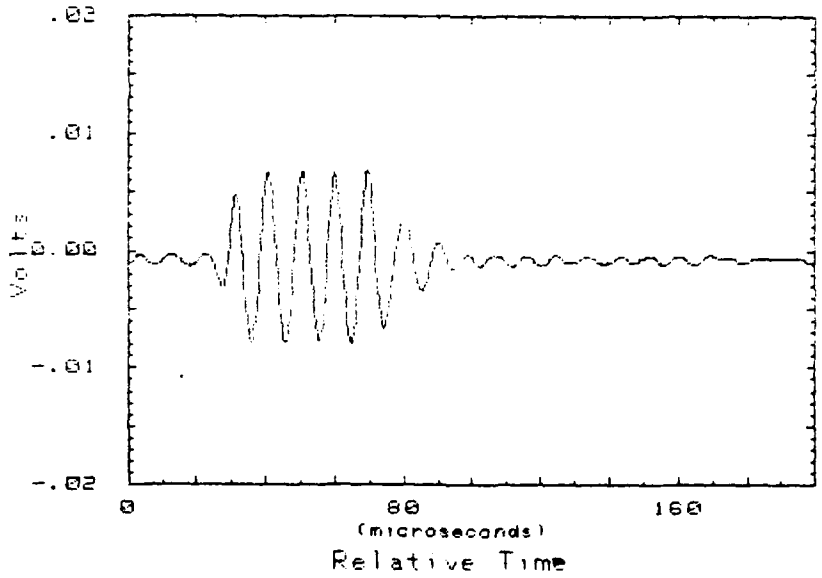

Figure 36. Styrofoam Sphere Reflection, 106 kHz N=5

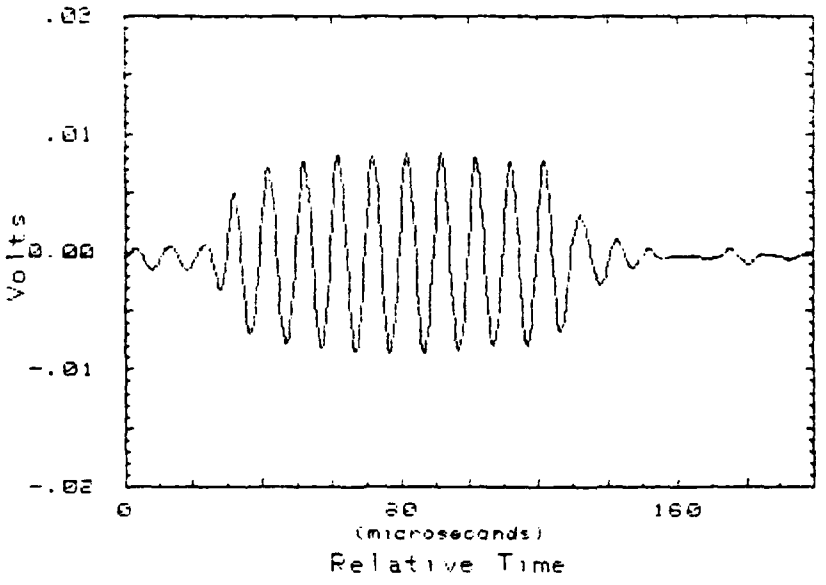

Figure 37. Styrofoam Sphere Reflection, 100 kHz N=10

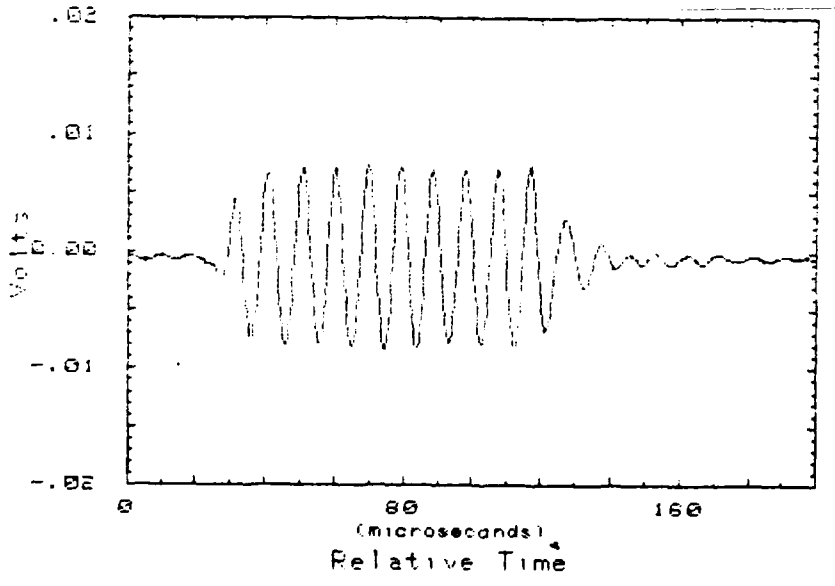

Figure 38. Styrofoam Sphere Reflection, 106 kHz N=10

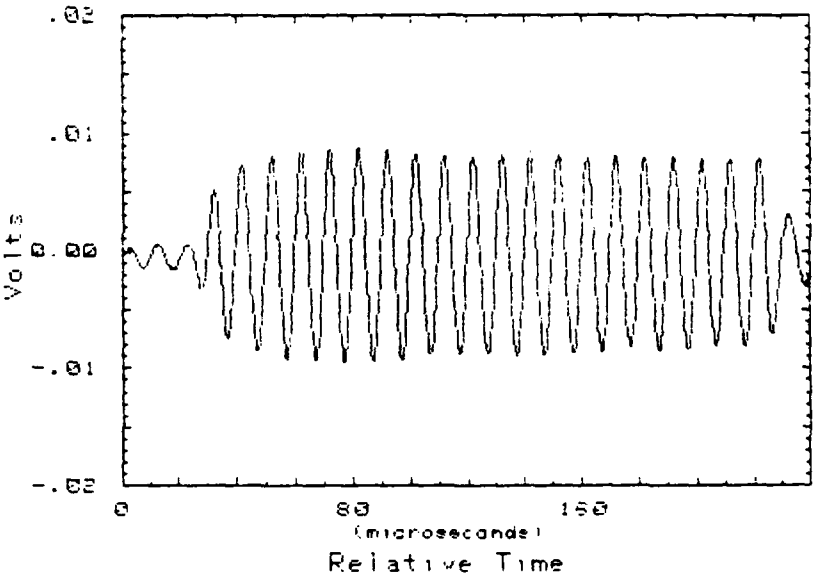

Figure 39. Styrofoam Sphere Reflection, 100 kHz N=20

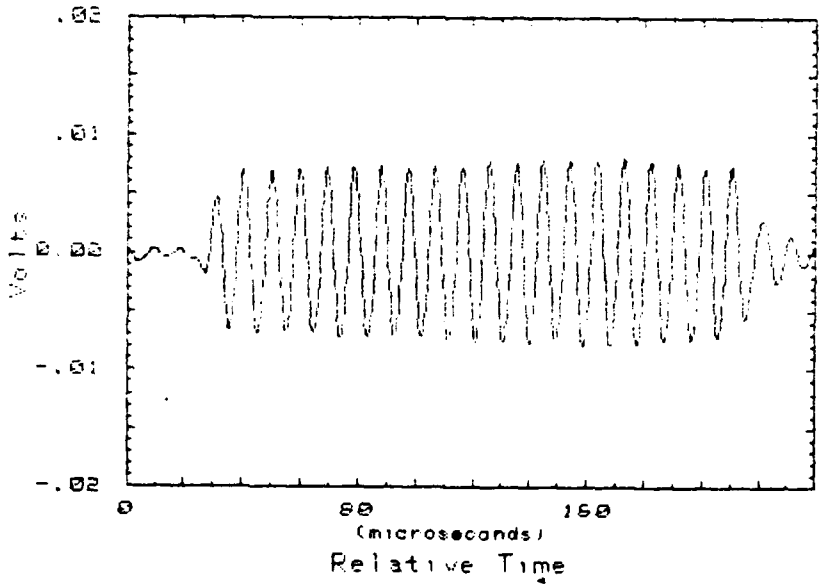

Figure 40. Styrofoam Sphere Reflection, 106 kHz N=20

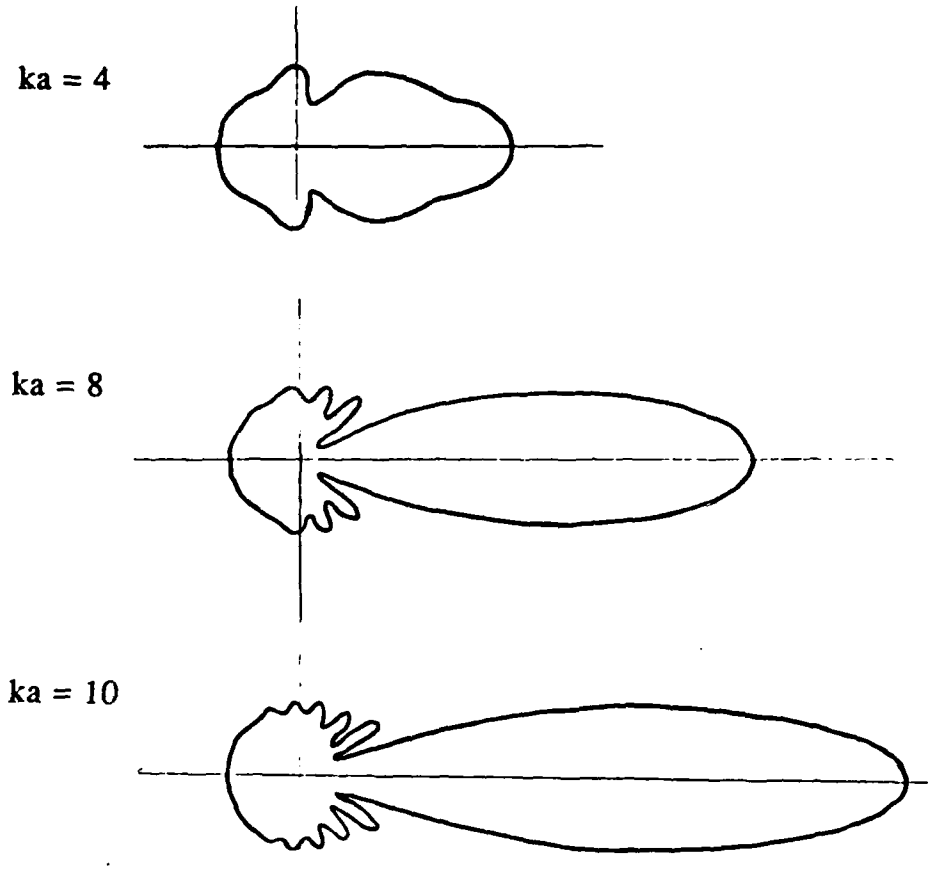

Figure 41. Theoretical Scattering Patterns for Rigid Spheres in Water

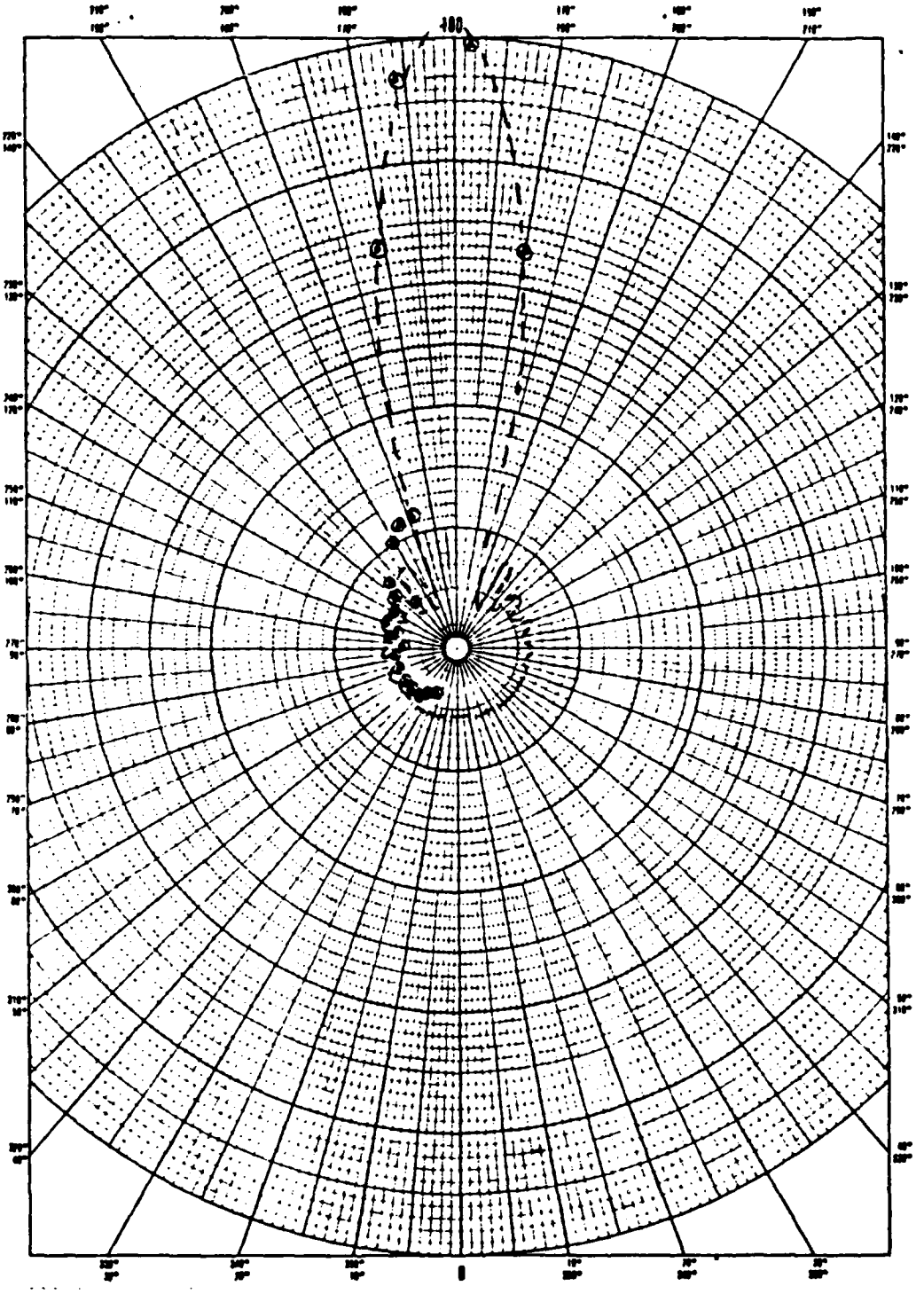

Figure 42. Bistatic Form Function of a Styrofoam Sphere ka = 10

VI. BISTATIC SCATTERING OF A STYROFOAM CYLINDER

A styrofoam cylinder of diameter 2.5 cm and length 20 cm with flat ends was used for bistatic scattering measurements. The particular diameter was chosen because the styrofoam was commercially available in that size. The length was selected using two criteria: (1) the length was small enough so that the receiver could be placed in the far field of the sound reflected from the cylinder and (2) it was large enough to clearly present a cylindrical shape.

Since the F41 was not omnidirectional, there was concern of approximating a plane wave at the target. The lower the frequency, the better the pressure distribution across the target because of the larger major lobe, but the wavelength-to-target length ratio would be less and the signal-to-noise ratio also became poorer at lower frequencies. A frequency of 70 kHz was chosen at a source-to-target distance of 125 cm. Figure 43 shows the incident pressure distribution as a function of distance off the axis at a distance of 125 cm. The lower curve is for the monostatic case where the receiver shadowed some of the incident energy with a receiver-to-target center distance of 50 cm. A two percent pressure amplitude difference existed for the shadowed case. An eight percent decrease in pressure amplitude existed when not shadowed.

The cylinder was mounted to a 1/8-inch diameter metal tube which had a 2 X 1/2 X 1/16-inch flat plate epoxied to it to provide a means of rotating the cylinder. The flat plate was forced into the interior of the cylinder and provided a snug fit. The effect of the plate on the reflections was assumed to be neglible since it was completely surrounded by the styrofoam. The tube was as small as possible to minimize reflections. A string with weights was attached to keep the styrofoam

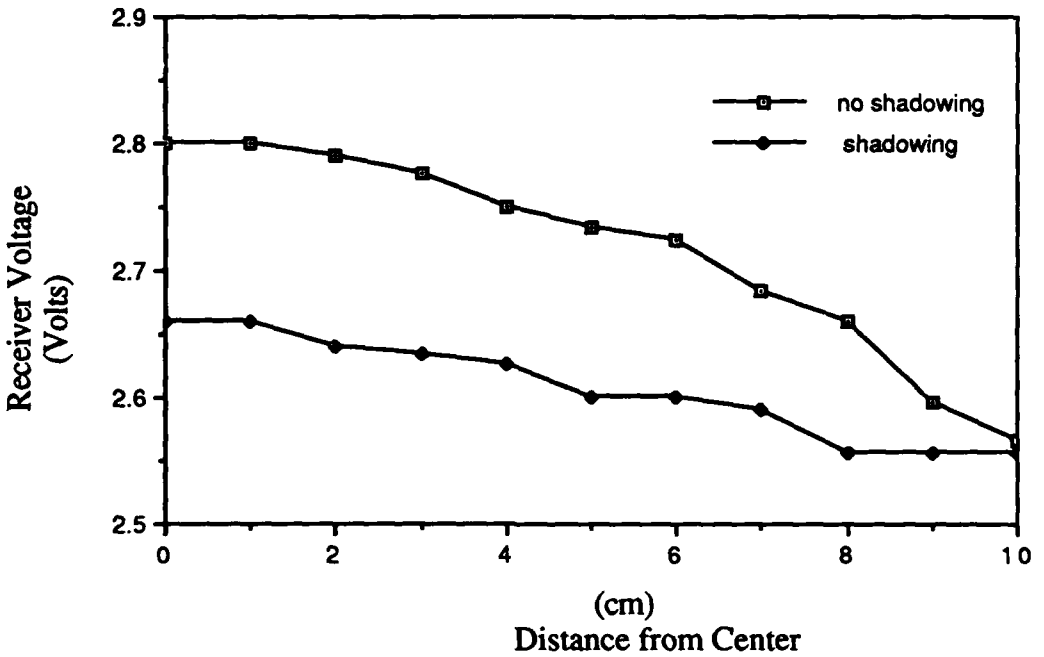

Figure 43. Pressure Distribution at 70 Khz

cylinder submerged. The thin tube was soldered into a 3/8-nch diameter tube which supported the entire arrangement. The cylinder was level before entering the water and appeared to remain that way when in the water. Figure 44 illustrates the support setup .

Data were recorded for nine bistatic angles. Time discrimination of the reflected pulse was used whenever possible. The source-to-receiver distance was 125 $\pm$ 2 cm in all cases with the F41 being driven at 177 V rms. The Ithaco preamplifier setting was 20X with a 3-300 kHz bandwidth. Receiver-to-cylinder center distance varied, but the receiver was always in the far field of the cylinder. All data were extrapolated to one meter from the target center for comparison. A 20 cycle pulse was used.

The cylinder was initially aligned broadside to the source by eye to within an uncertainty of about $\pm$ 4 degrees. Assuming symmetry, data were taken for 180 degrees of rotation and several points were taken beyond t hat limit. Figure 45

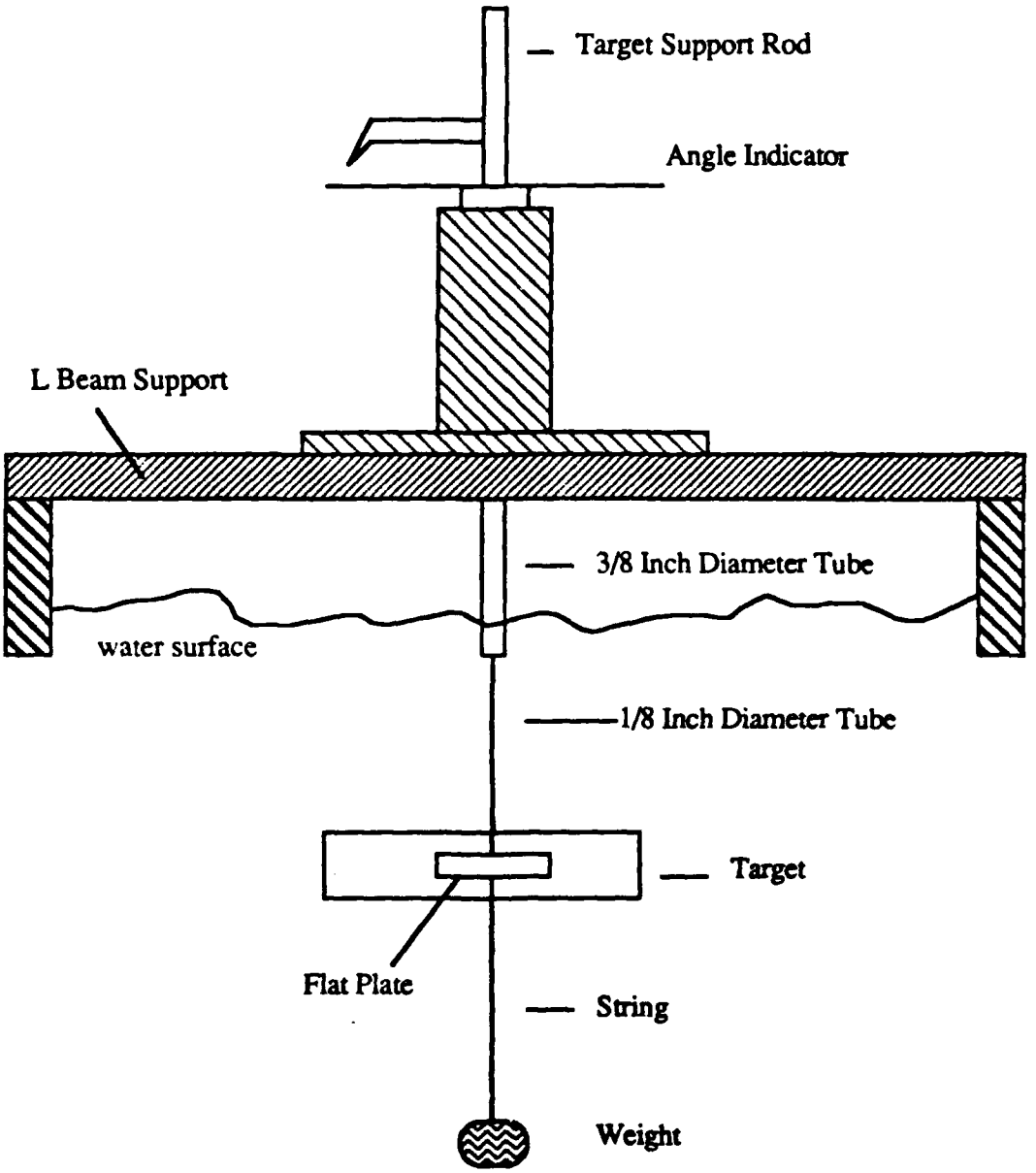

Figure 44. Support Platform Setup

illustrates the angles measured in the experiments. The varied angle, A, is the angle made between the cylinder's normal and the line connecting the center of the target to the source axis. Angle B is the bistatic angle.

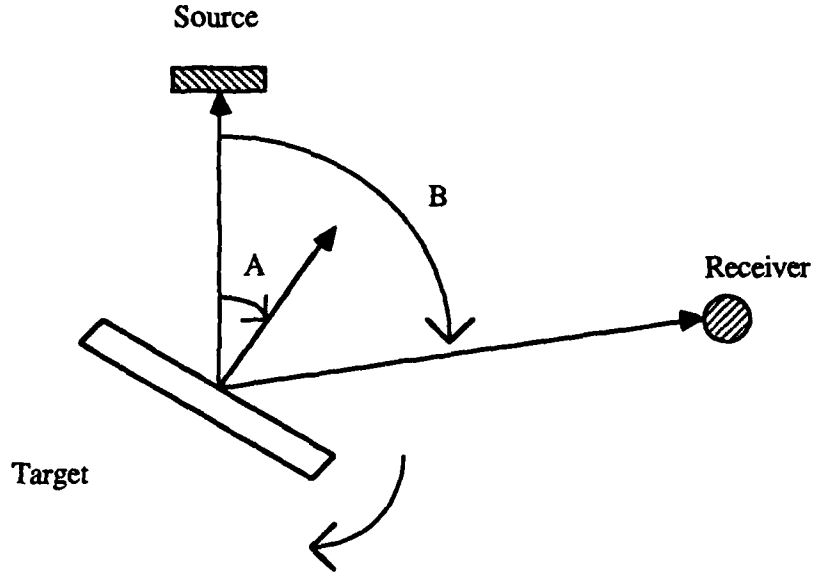

Figure 45. Measured Angles in Experiment

The results of the experiment are shown in Figures 46 to 55. In most cases, strong peaks were observed when angle A was one-half the bistatic angle and secondary peaks with smaller amplitude occurred 90 degrees from that. This geometry seems to indicate specular reflection off the long cylinder's surface and its flat ends respectively. As the bistatic angle increases the secondary peak broadens and eventually disappears. Well into the forward scattering region, greater than 150 degrees of bistatic angle, the data became less predictable The distinction of the primary and secondary peaks became less clear with additional peaks showing up. At a bistatic angle of 180 degrees no distinctive peaks were present and amplitude became very large in comparison to other bistatic angles.

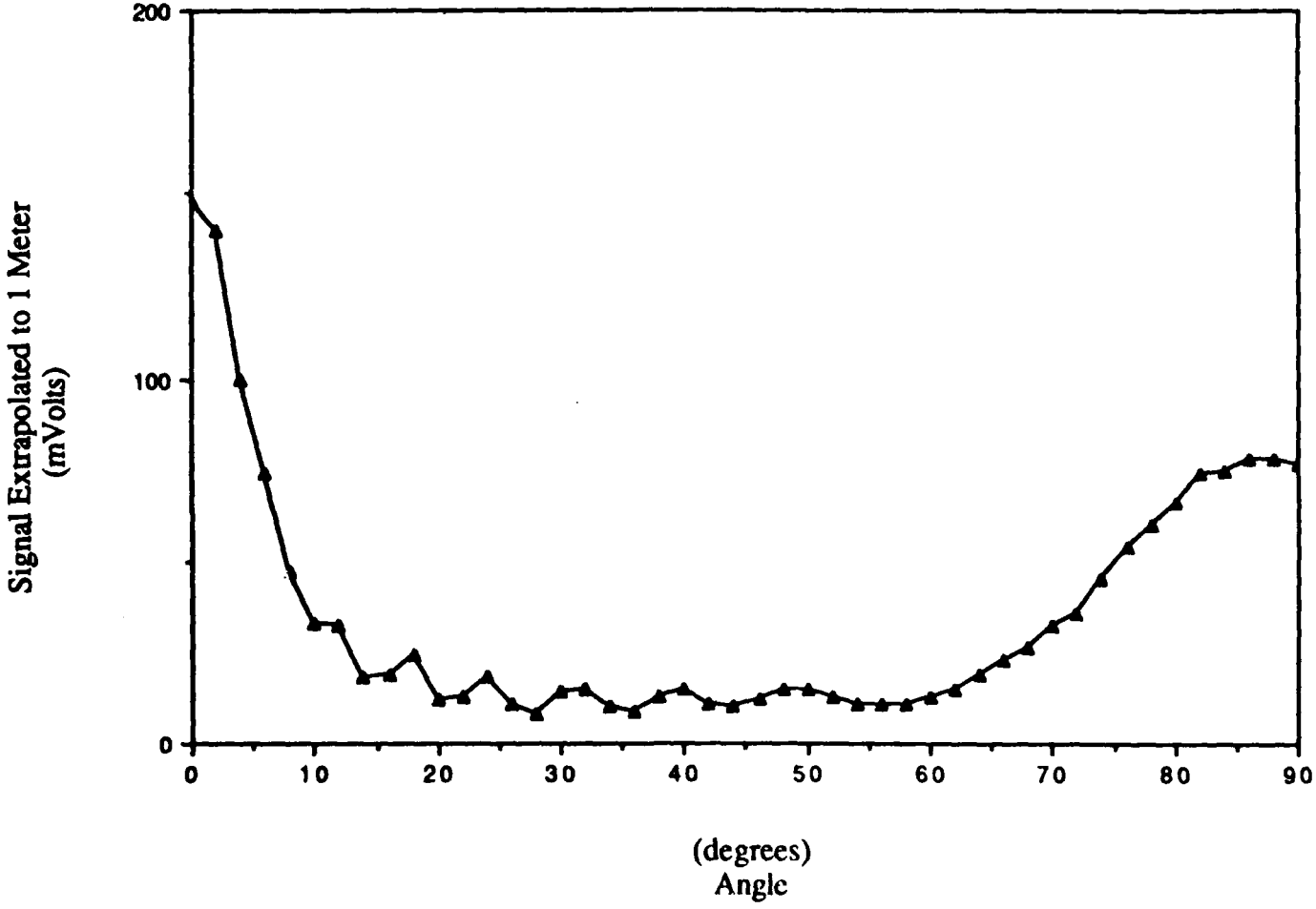

Figure 46. Styrofoam Cylinder, Backscattered, 70 kHz

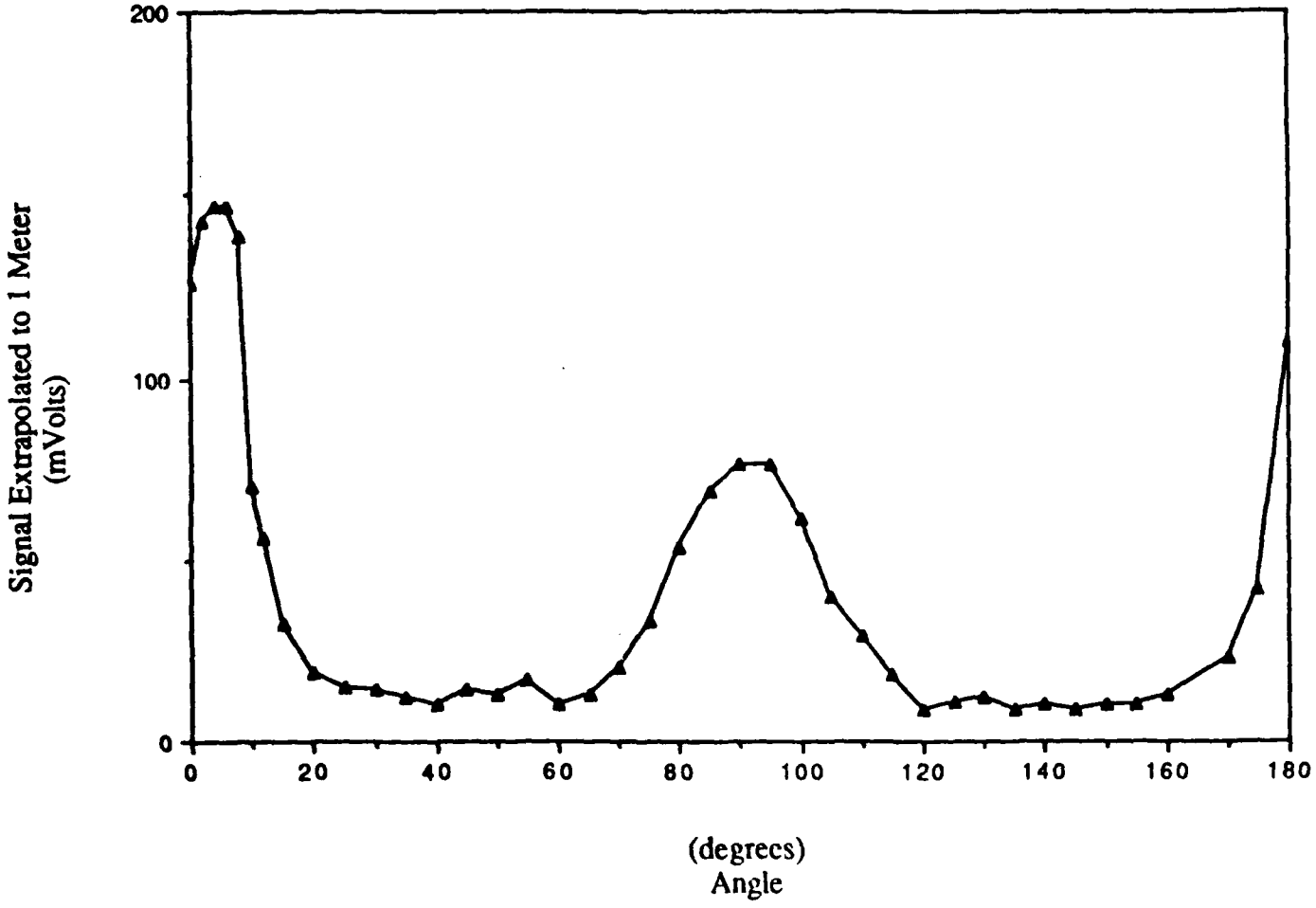

Figure 47. Styrofoam Cylinder, Bistatic Angle 10 Degrees, 70 kHz

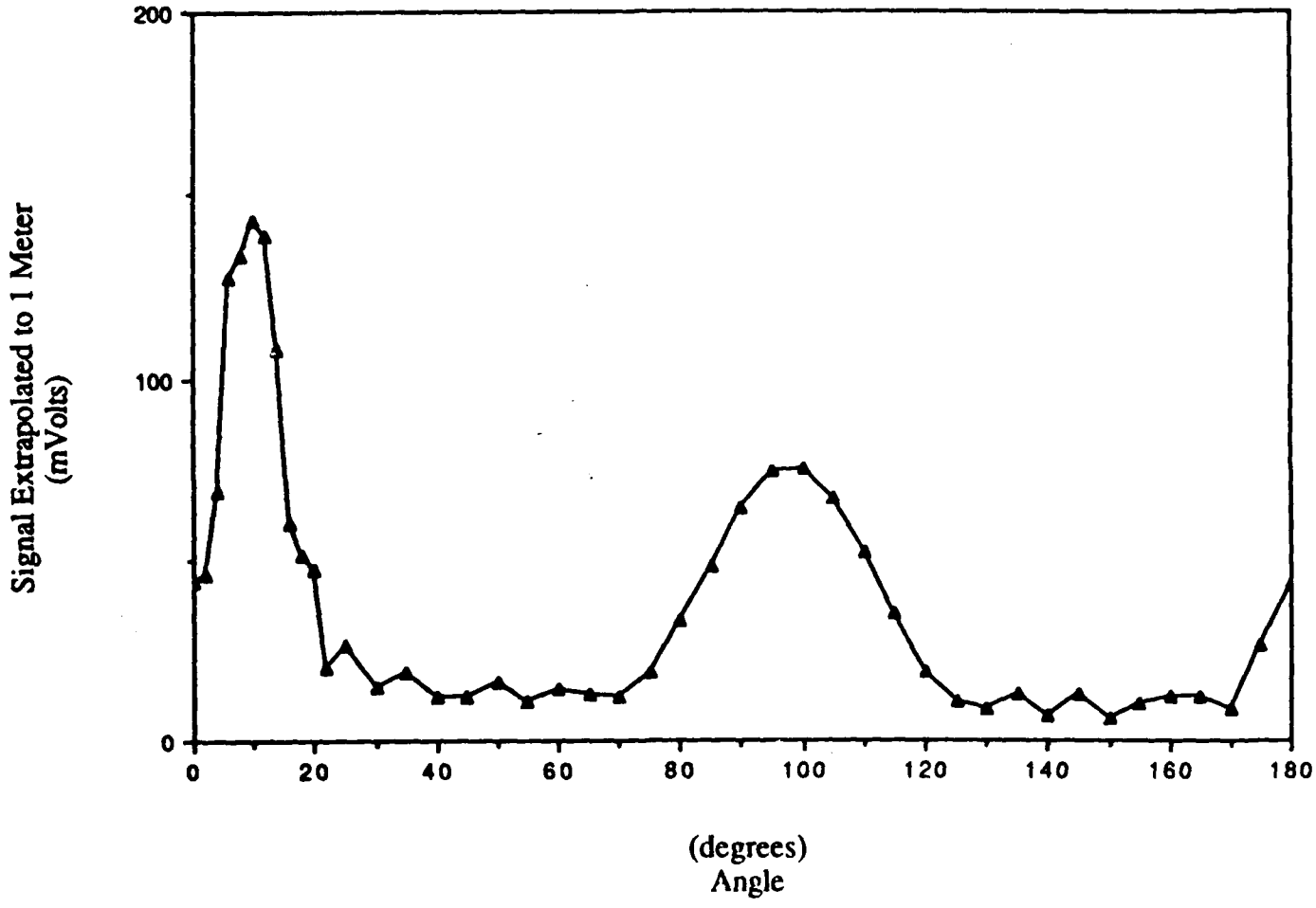

Figure 48. Styrofoam Cylinder, Bistatic Angle 20 Degrees, 70 kHz

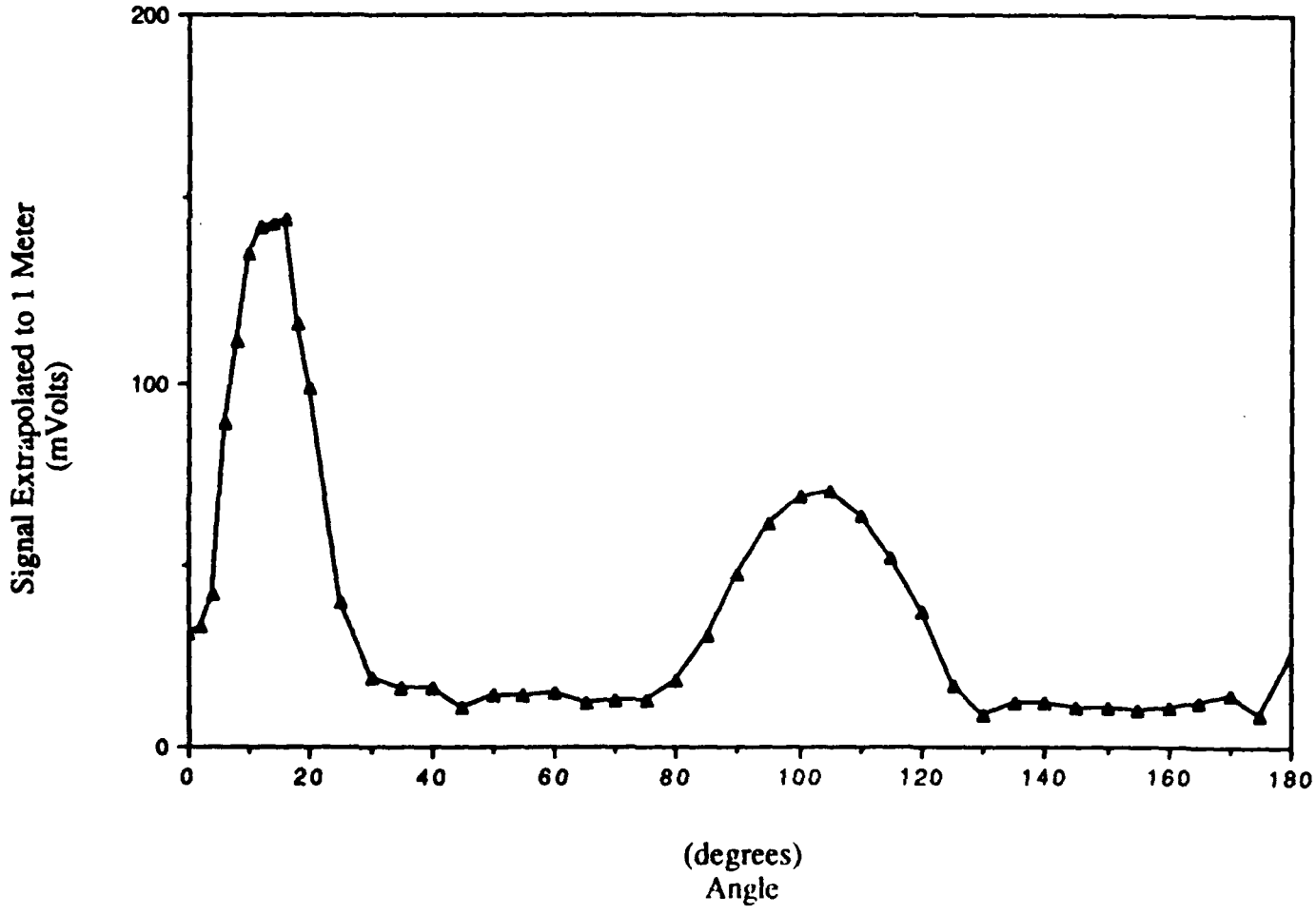

Figure 49. Styrofoam Cylinder, Bistatic Angle 30 Degrees, 70 kHz

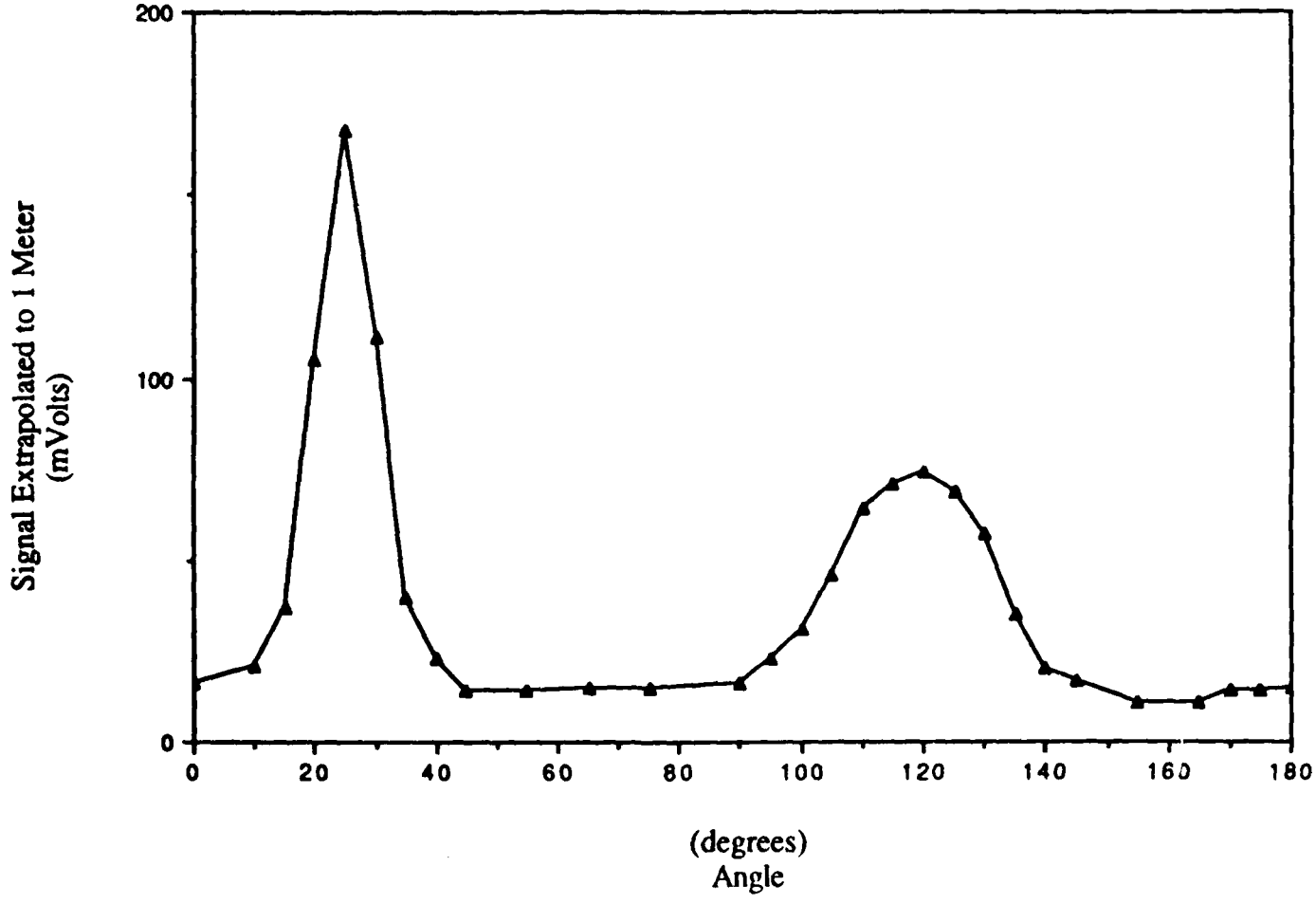

Figure 50. Styrofoam Cylinder, Bistatic Angle 50 Degrees, 70 kHz

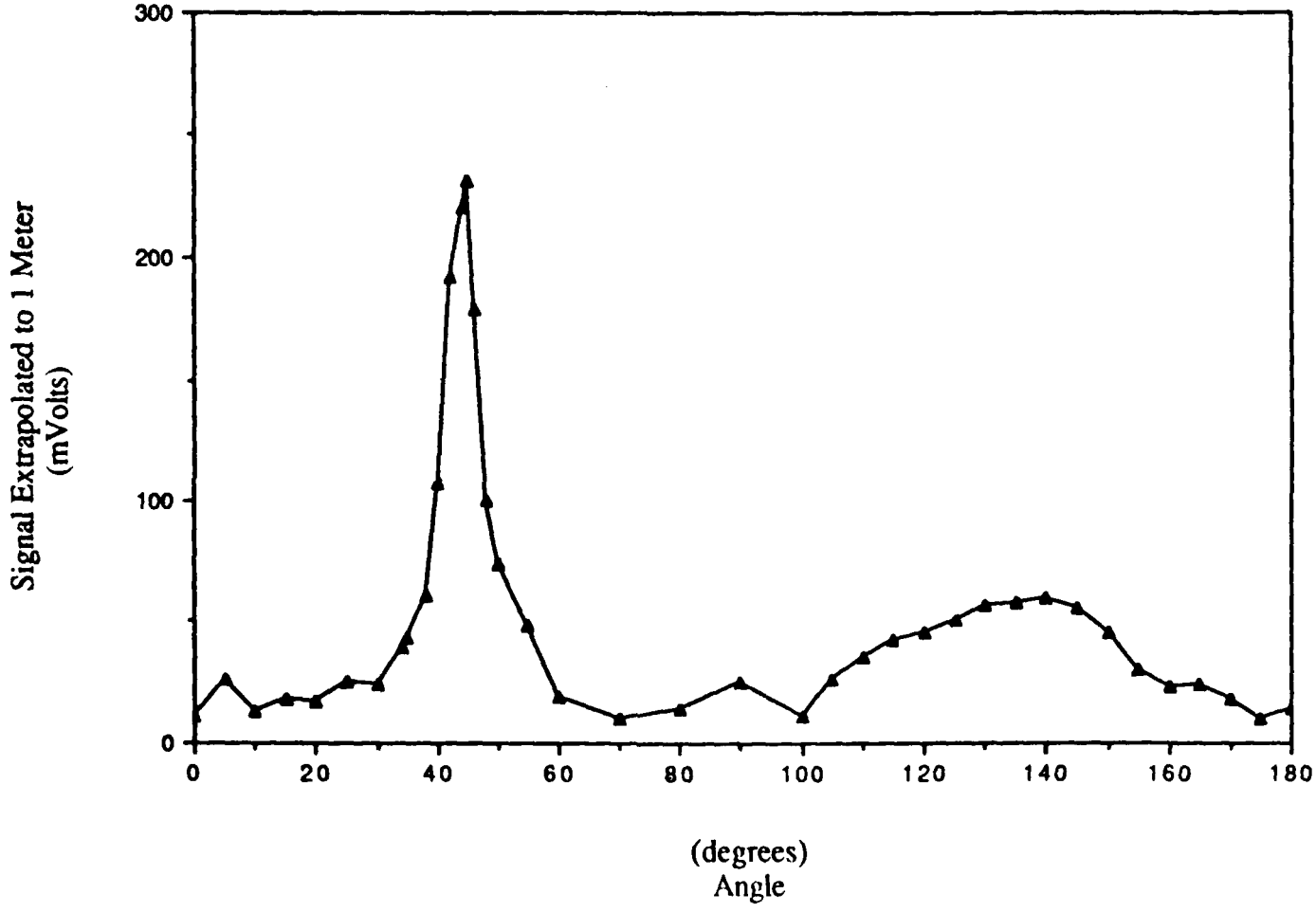

Figure 51. Styrofoam Cylinder, Bistatic Angle 90 Degrees, 70 kHz

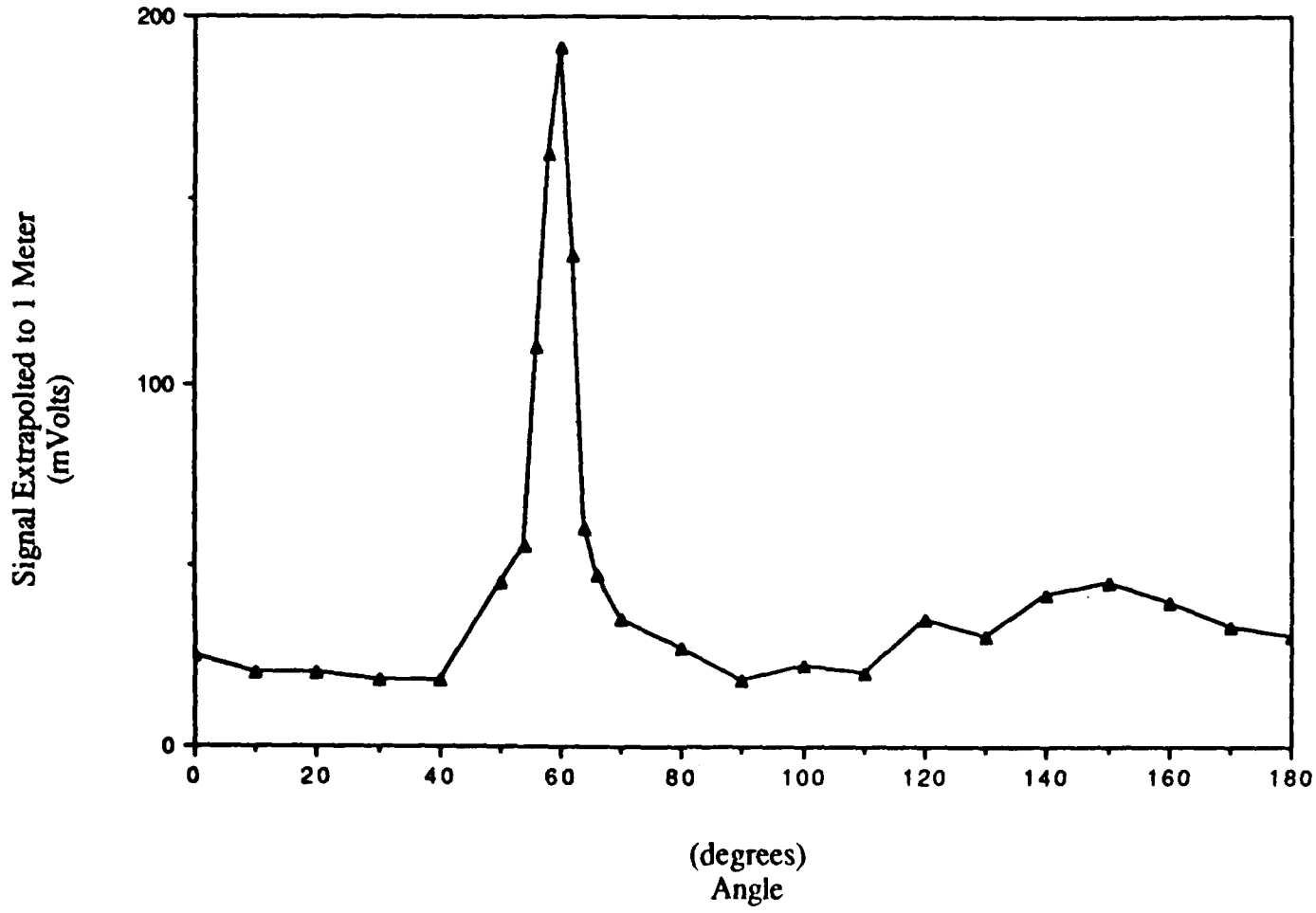

Figure 52. Styrofoam Cylinder, Bistatic Angle 120 Degrees, 70 kHz

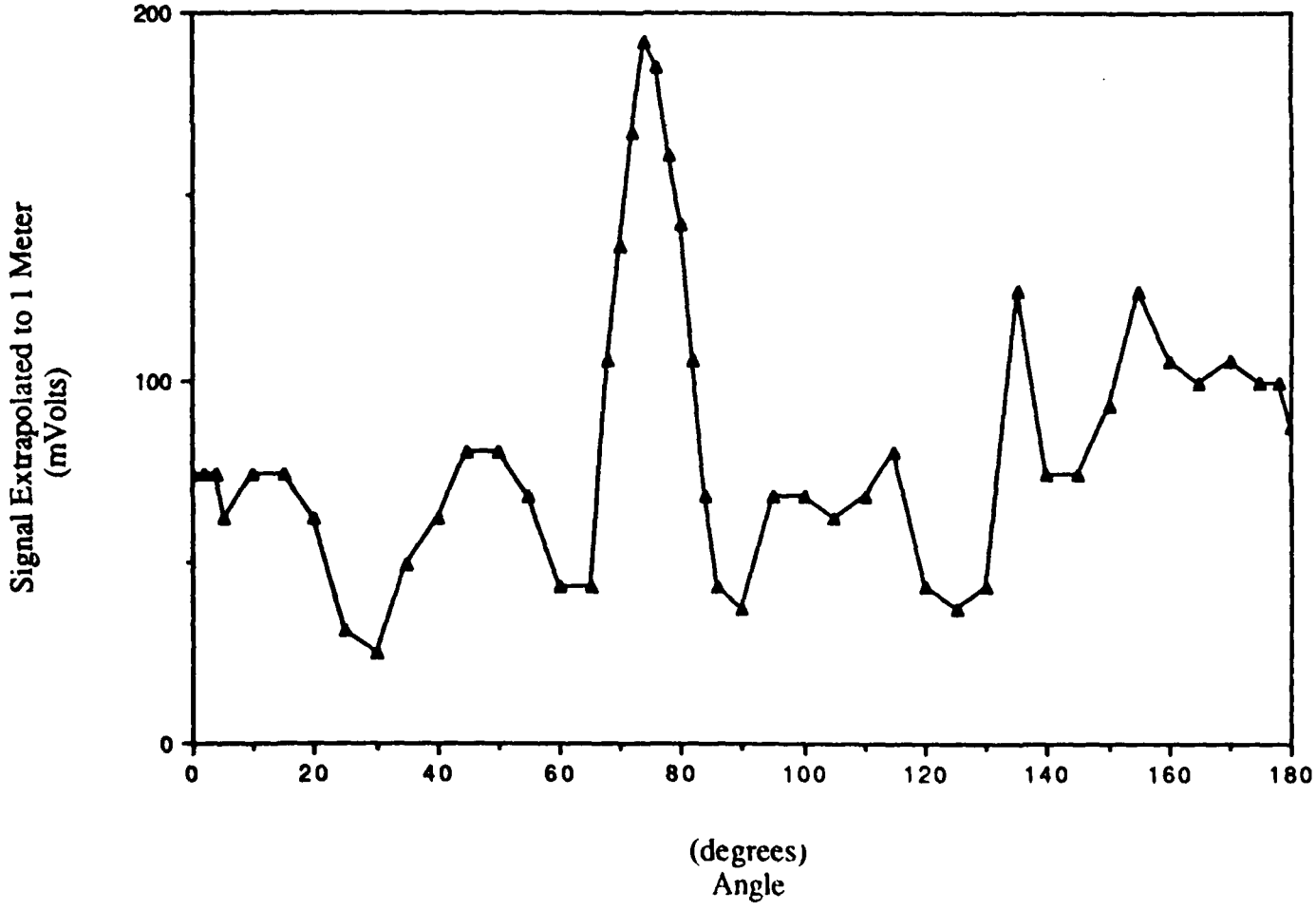

Figure 53. Styrofoam Cylinder, Bistatic Angle 150 Degrees, 70 kHz

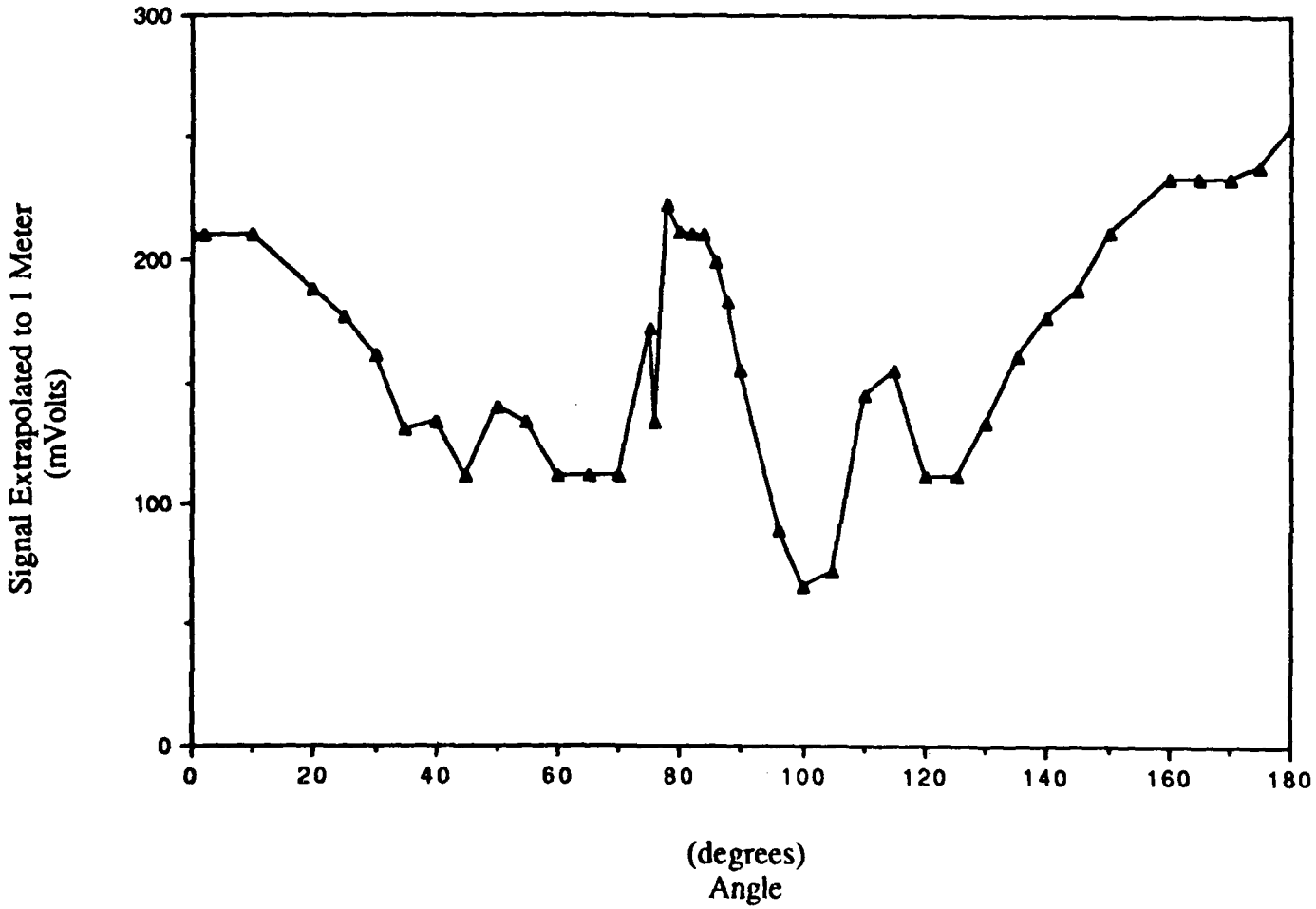

Figure 54. Styrofoam Cylinder, Bistatic Angle 165 Degrees, 70 kHz

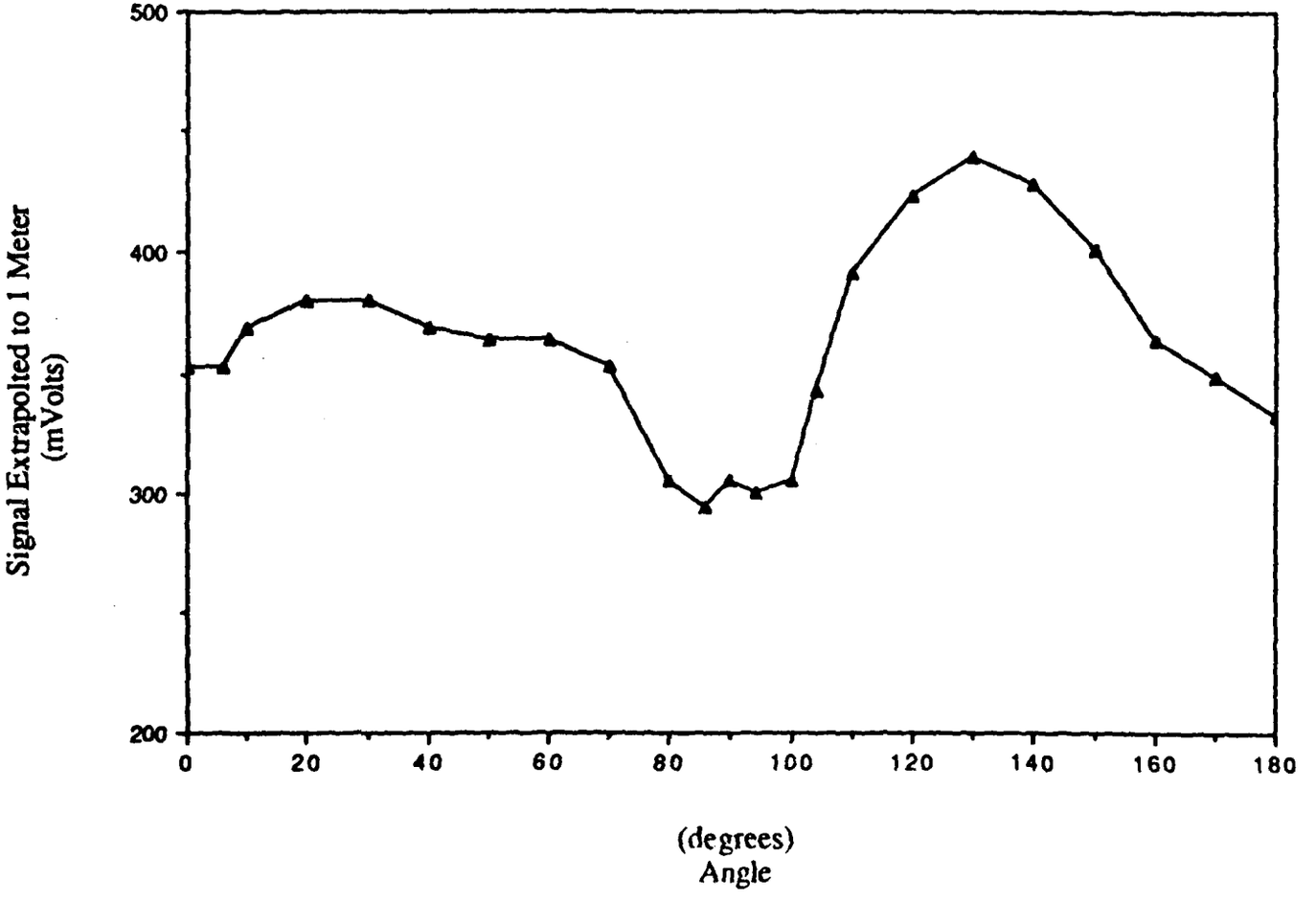

Figure 55. Styrofoam Cylinder, Bistatic Angle 180 Degrees, 70 kHz

VII. CONCLUSION AND RECOMMENDATIONS

A data acquisition system using the Tektronix 2430 digital oscilloscope was implemented to extract scattered waveforms in a noise-filled water environment. The system was verified to work and reflected waveforms were collected. Preliminary work revealed that the relative movement of the source and receiver between collection of waveforms was critical in obtaining accurate data using a digital sampling system with a subtraction routine. Data collection was slow and tedious.

Several aspects influencing scattered waveforms, including target composition, frequency, and pulse length were observed and recorded. The effects of these on the waveforms of the reflected pulse produce difficutlies in measuring the intensity of pulses with waveforms not identical of the incident pulse.

Styrofoam targets were used to circumvent the problem of waveform dependence on frequency, pulse length, and composition. Bistatic measurements were taken using a sphere and a cylinder as targets. The data from the sphere compared well with theoretical predictions for a perfectly reflecting sphere. Readily available data were not found for comparison with the results obtained for the cylinder. The goal of matching wavelength-to-target length ratios observed in oceanic conditions was not done in this work. The USRD type E27 transducer would be an excellent source for this application since it has a frequency range 100 to 500 kHz. Its small size makes its beamwidths very large which is beneficial when receiver-target distance is limited by tank dimensions. The E27 is also very lightweight and easily moved. The effect of the jitter would have to be evaluated at the higher frequencies.

The bistatic radar cross-section theorem could not be compared to the data collected in this report. The wavelengths used in the experiments are not close to the "vanishing limit" as stated in the theorem. One common trend between the bistatic data and the theorem was that the data became less predictable as the bistatic angle approached 180 degrees.

For future work, a physical structure must be made to facilitate positioning of the source, target and receiver in three dimensions so that data collection can be completely automated and accuracy improved. The rotation of supports should have a digital device to allow control by the computer. The design and construction of such a system would not be a trivial project and would require a great amount of ingenuity and experience with electronic devices. The payoff of having such a system would be great to students studying underwater acoustics and in particular to anyone studying scattering effects. Once a positioning system is built and completely automated, data collection will become simpler and more time can be devoted to analyzing it.

APPENDIX A
COMPUTER LISTING OF "TEX"

```
40    !#####################################################################
50    !
60    !PROGRAM TEX
70    !
80    !
90    !        DATA AQUISITION FOR BI-STATIC TARGET STRENGTHS
100   !        USING THE TEXTRONIX 2430 DIGITAL OSCILLOSCOPE
110   !
120   !        THIS PROGRAM TRANSFERS WAVEFORM DATA FROM THE TEX 2430
130   !        TO THE COMPUTER WHERE IT IS CONVERTED TO ACTUAL VOLTAGE
140   !        VALUES AND STORED ON A FLEXIBLE DISK.  INPUT FROM THE
150   !        USER REQUIRES FILE NAME, DESCRIPTION, AND CONTINUATION
160   !        RESPONSES.  PREVIOUS SETUP OF THE TEX 2430 IS REQUIRED.
170   !        A THOROUGH KNOWLEDGE OF THE GPIB CODES IS NECESSARY. SEE
180   !        THE OPERATOR'S MANUAL AND THE INTERFACING MANUAL FOR
190   !        THE TEX 2430.
200   !
210   !#####################################################################
220   !                        INITIALIZATION
240   !#####################################################################
250   PRINTER IS CRT
260   OPTION BASE 0
270   DIM Vdata$[15],W$[40]!NAME OF DATA FILE AND DESCRIPTION
280   DIM A$[200],B$[5000],D$[5]!PRE-WAVEFORM AND WAVEFORM STRINGS
290   DIM V(1023),Tim(1023),Volt(1023)!DATA ARRAYS
300   DIM X$[10],Ys$[10],Vs$[10],Ts$[10]
310   DIM An$[1]
320   !
330   !#####################################################################
340   !              TEXTRONIX SETUP
350   !#####################################################################
360   !
370   OUTPUT 704;"PATH OFF"!SHORTENS THE DATA STRING SENT BY THE 2430
380   !
390   !#####################################################################
400   !                    INPUT FROM USER
410   !#####################################################################
420   !
430   INPUT "NAME OF THE DATA FILE?",Vdata$
440   INPUT "DOES FILE ALREADY EXIST?(Y=YES)",An$
450   IF An$="Y" THEN PURGE Vdata$
460   INPUT "INPUT FILE DESCRIPTION?(40 CHARACTERS MAX)",W$
470   BEEP
480   PRINT "ALLOWING DATA DISK INSERTION. PRESS CONTINUE TO RESUME."
490   PAUSE
```

```
500   CREATE BDAT Vdata$,1,17000
510   ASSIGN @Dfile TO Vdata$
520   PRINT
530   !
540   !#####################################################################
550   !              OBTAIN WAVEFORM
560   !#####################################################################
570   !
580   PRINT "OBTAIN DESIRED WAVEFORM ONTO TEXTRONIX"
590   PRINT "PRESS CONTINUE TO RESUME"
600   PAUSE
610   !
620   !#####################################################################
630   !           RECEIVING PRE-WAVEFORM DATA AND THE WAVEFORM
640   !#####################################################################
650   !
660   OUTPUT 704;"WFM? XIN"!TIME INCREMENT BETWEEN POINTS
670   ENTER 704;X$
680   OUTPUT 704;"WFM? YMU"!VOLTAGE DIGITIZING INCREMENT
690   ENTER 704;Ys$
700   OUTPUT 704;"CH1? VOL"!VOLTS/DIV
710   ENTER 704;Vs$
720   OUTPUT 704;"HOR? BSE"!B TIME SCALE
730   ENTER 704;Ts$
740   !
750   !
760   OUTPUT 704;"CURV?"
770   ENTER 704;B$
780   !
790   !#####################################################################
800   !          SEPARATION OF ASCII STRING INTO DATA POINTS
810   !#####################################################################
820   !
830   N=LEN(B$)
840   D$=""
850   Inc=0
860   !
870   FOR I=1 TO N
880   IF B$[I,I]="," THEN
890   V(Inc)=VAL(D$)
900   Inc=Inc+1
910   D$=""
920   GOTO 950
930   END IF
940   D$=D$&B$[I,I]
950   NEXT I
960   !
970   !#####################################################################
980   !                  CONVERSION TO REAL-TIME DATA
990   !#####################################################################
1000  !
```

```
1010  ! X$=TIME INCREMENT BETWEEN POINTS  DIV/50
1020  ! YS$=VOLTS BETWEEN POINTS  DIV/25
1030  ! VS$=VOLTS/DIV
1040  ! TS$=B TRIGGER TIME SCALE
1050  !
1060  Deltim=VAL(X$)
1070  Delvol=VAL(Ys$)
1080  Vscale=VAL(Vs$)
1090  Tscale=VAL(Ts$)
1100  !
1110  OUTPUT @Dfile;W$,Tscale,Vscale
1120  FOR I=0 TO 1023
1130  Tim(I)=I*Deltim
1140  Volt(I)=V(I)*Delvol
1150  NEXT I
1160  !
1170  PRINT "WRITING TO FILE"
1180  OUTPUT @Dfile;Tim(*),Volt(*)
1190  ASSIGN @Dfile TO *
1200  BEEP
1210  !
1220  !#########################################################################
1230  !
1240  INPUT "DO YOU WANT ANOTHER WAVEFORM? Y=YES",An$
1250  IF An$="Y" THEN GOTO 430
1260  !
1270  PRINT "PROGRAM TERMINATED"
1280  END
```

APPENDIX B
COMPUTER LISTING OF "PLOT"

```
10    !PROGRAM: PLOT
20    !
30    !   THIS PROGRAM TAKES TWO FORMATTED BDAT FILES AND SUBTRACTS
40    !   ONE FROM THE OTHER.  IT WAS DESIGNED FOR USE USING WAVEFORMS
50    !   OBTAINED ON THE TEXTRONIX 2430 DIGITAL OSCOPE.  DATA IS TAKEN
60    !   FROM THE FILES IN THE FOLLOWING ORDER.
70    !
80    !            W$ = FILE DESCRIPTION STRING
90    !            TSCALE = TIME SCALE OF THE SCOPE (SEC/DIV)
100   !            VSCALE = VOLTAGE SCALE OF THE SCOPE (VOLT/DIV)
110   !            T(0-1023) = TIME ARRAY (SEC)
120   !            V(0-1023) = VOLTS ARRAY (VOLTS)
130   !
140   !   THE SUBTRACTION RESULTS ARE THEN ABLED TO BE PLOTTED AS HARD
150   !   COPY ON THE THINK JET OR PEN PLOTTER. A STANDARD OPTION IS
160   !   INCORPORATED  FOR EASE WHEN USING THE PROGRAM FREQUENTLY WITH
170   !   THE SAME PARAMETERS.  THE PROGRAM ALLOWS FLEXIBILITY IN
180   !   CHANGING THE PLOT'S PARAMTERS BEFORE THE HARD COPY.
190   !
200   !#########################################################################
210   !          INITIALIZATION
220   !#########################################################################
230   !
240   OPTION BASE 0
250   DIM X_data(1023),Y_data(1023),Y_axis_units$[32]
260   DIM Head_lbl$[60],Y_axis_lbl$[60],X_axis_lbl$[32]
270   DIM X_axis_units$[32],Clear_crt$[2],C$[2],Sub_head_lbl$[32]
280   DIM X_char$[8],Vdata$[15],W$[40],Vdata2$[15],Y_char$[8]
290   DIM X1(1023),Y1(1023),X2(1023),Y2(1023)
300   Clear_crt$=CHR$(255)&CHR$(75)
310   C$=CHR$(255)&"K"
320   !
330   !#########################################################################
340   !
350   GOSUB Load_file
360   INPUT "DO YOU WISH TO USE THE STANDARD PARAMETERS? Y=YES",Dec2$
370   IF Dec2$="Y" THEN
380       GOSUB Stand_params
390       GOTO 420
400   END IF
410   GOSUB Initial_params
420   A$="N"
430   GOSUB Plot_data
440   INPUT "WISH TO CHANGE CURRENT GRAPHICS PARAMETERS? Y=YES",Dec2$
450   IF Dec2$="Y" THEN GOSUB Change_params
```

```
460   INPUT "ANOTHER DATA FILE PLOTTED ON SAME HARD COPY GRAPH?",Dec6$
470   WHILE Dec6$="Y"
480     GOSUB Load_file
490     INPUT "LINE TYPE(1=SOLID,4=DASH,5=BIG DASH,6=DASH-DOT",Line_num
500     INPUT "PEN NUMBER 1 TO 8",Pen_num
510     GOSUB Same_graph
520     GOTO 460
530   END WHILE
540   INPUT "DO YOU WISH TO CHANGE ANY MORE PARAMTERS? Y=YES",Dec2$
550   IF Dec2$="Y" THEN GOTO 450
560   INPUT "DO YOU WISH TO DUMP GRAPHICS? Y=YES",A$
570   IF A$="Y" THEN GOSUB Plot_data
580   INPUT "DO YOU WANT TO PLOT A DIFFERENT GRAPH? Y=YES",Dec7$
590   IF Dec7$="Y" THEN GOTO 350
600   GOSUB End_program
610   !
620   !###########################################################################
630   !                STANDARD PARAMETERS
640   !###########################################################################
650   !
660 Stand_params:  !
670   Head_lbl$=W$
680   Sub_head_lbl$=Vdata$
690   X_char$="K"
700   Y_char$="DD.DD"
710   Y_axis_lbl$="Volts"
720   X_axis_lbl$="Relative Time"
730   Y_axis_units$="Volts"
740   X_axis_units$="microseconds"
750   Left=0
760   Right=19*Tscale
770   Bottom=-Vscale*4
780   Top=Vscale*4
790   X_tic_sp=Tscale/2
800   Y_tic_sp=Vscale/5
810   X_maj_ct=2
820   Y_maj_ct=5
830   Maj_tic=2
840   Xgridtic=Tscale
850   Ygridtic=Vscale
860   Xgridmaj=1
870   Ygridmaj=1
880   Majgrid_sz=2
890   Y_incmt=2*Vscale
900   X_incmt=4*Tscale
910   Line_num=1
920   RETURN
930   !
940   !###########################################################################
950   !                INITIAL PARAMETERS
960   !###########################################################################
```

```
970   !
980 Initial_params:   !
990   X_tic_so=0
1000  Y_tic_sp=0
1010  X_maj_ct=1
1020  Y_maj_ct=1
1030  Maj_tic=2
1040  Xgridtic=0
1050  Ygridtic=0
1060  Xgridmaj=1
1070  Ygridmaj=1
1080  Majgrid_sz=2
1090  INPUT "GRAPH HEADING LABEL,32 CHAR. MAX",Head_lbl$
1100  INPUT "GRAPH SUB LABEL,32 CHAR. MAX",Sub_head_lbl$
1110  INPUT "IMAGE FOR X AXIS NUMERICS, 8 CHAR. MAX",X_char$
1120  INPUT "IMAGE FOR Y AXIS NUMERICS, 8 CHAR. MAX",Y_char$
1130  INPUT "Y AXIS LABEL,32 CHAR. MAX",Y_axis_lbl$
1140  INPUT "X AXIS LABEL,32 CHAR. MAX",X_axis_lbl$
1150  INPUT "Y AXIS UNITS,32 CHAR. MAX",Y_axis_units$
1160  INPUT "X AXIS UNITS,32 CHAR. MAX",X_axis_units$
1170  DISP "WINDOW LOOKED AT,LEFT,RIGHT,BOTTOM,TOP";
1171  INPUT Left,Right,Bottom,Top
1180  INPUT "X AXIS TICK SPACING,DEF=0(NO TICKS)",X_tic_sp
1190  INPUT "Y AXIS TICK SPACING,DEF=0(NO TICKS)",Y_tic_sp
1200  INPUT "NUM TIC INTVLS BTWN MAJ TICS X-DIR,DEF=1",X_maj_ct
1210  INPUT "NUM TIC INTVLS BTWN MAJ TICS Y-DIR,DEF=1",Y_maj_ct
1220  INPUT "SIZE OF MAJOR TICKS,DEF=2",Maj_tic
1230  INPUT "GRID X-TIC SPACING,DEF=0(NO TICKS)",Xgridtic
1240  INPUT "GRID Y-TIC SPACING,DEF=0(NO TICKS)",Ygridtic
1250  INPUT "NUM TICKS BTWN MAJOR TICKS Y-DIR,DEF=1",Ygridmaj
1260  INPUT "NUM TICKS BTWN MAJOR TICKS X-DIR,DEF=1",Xgridmaj
1270  INPUT "SIZE OF MAJOR GRID TICKS,DEF=2",Majgrid_sz
1280  INPUT "Y-AXIS INCREMENT",Y_incmt
1290  INPUT "X-AXIS INCREMENT",X_incmt
1300  DISP "LINE TYPE(1=SOLID,4=DASH,5=BIG DASH,6=DASH-DOT)";
1301  INPUT Line_num
1310  !
1320  RETURN
1330  !
1340  !##########################################################################
1350  !                LOAD DATA FILE
1360  !##########################################################################
1370  !
1380 Load_file:   !
1390  !
1400  INPUT "INPUT NAME OF DATA FILE 1",Vdata$
1410  INPUT "INPUT NAME OF DATA FILE 2 ",Vdata2$
1420  ASSIGN @Df1 TO Vdata$
```

```
1430  ENTER @Df1;W$,Tscale,Vscale,X1(*),Y1(*)
1440  ASSIGN @Df1 TO *
1450  ASSIGN @Df2 TO Vdata2$
1460  ENTER @Df2;W$,Tscale,Vscale,X2(*),Y2(*)
1470  ASSIGN @Df2 TO *
1480  MAT X_data= X1
1490  MAT Y_data= Y1-Y2
1500  PRINT "DATA FILES READ"
1510  BEEP
1520  RETURN
1530  !
1540  !#########################################################################
1550  !                      PLOT DATA
1560  !#########################################################################
1570  !
1580 Plot_data:  !
1590  !
1600  IF A$="Y" THEN
1610     OUTPUT KBD;Clear_crt$;
1620     GINIT
1630     PLOTTER IS CRT,"INTERNAL"
1640     GOTO 1770
1650  END IF
1660  INPUT "IS THIS TO BE A HARDCOPY PLOT? Y=YES",Dec1$
1670  IF Dec1$="Y" THEN
1680     GINIT
1690     PLOTTER IS 705,"HPGL"
1700     GOTO 1770
1710  ELSE
1720     OUTPUT KBD;Clear_crt$;
1730     GINIT
1740     PLOTTER IS CRT,"INTERNAL"
1750     GOTO 1770
1760  END IF
1770  GRAPHICS ON
1780  PEN 1
1790  X_gdu_max=100*MAX(1,RATIO)
1800  Y_gdu_max=100*MAX(1,1/RATIO)
1810  LORG 5
1820  CSIZE 4
1830  MOVE .48*X_gdu_max,.93*Y_gdu_max
1840  LABEL Head_lbl$
1850  MOVE .48*X_gdu_max,.89*Y_gdu_max
1860  CSIZE 3
1870  LABEL Sub_head_lbl$
1880  DEG
1890  LDIR 90
1900  CSIZE 4
```

```
1910  MOVE .04*X_gdu_max,.55*Y_gdu_max
1920  LABEL Y_axis_lbl$
1930  LORG 5
1940  LDIR 0
1950  MOVE .48*X_gdu_max,.15*Y_gdu_max
1960  CSIZE 4
1970  LABEL X_axis_lbl$
1980  MOVE .48*X_gdu_max,.19*Y_gdu_max
1990  CSIZE 3
2000  LABEL "(";X_axis_units$;")"
2010  MOVE .70*X_gdu_max,.74*Y_gdu_max
2020  VIEWPORT .15*X_gdu_max,.85*X_gdu_max,.25*Y_gdu_max,.86*Y_gdu_max
2030  WINDOW Left,Right,Bottom,Top
2040  AXES X_tic_sp,Y_tic_sp,Left,Bottom,X_maj_ct,Y_maj_ct,Maj_tic
2050  AXES X_tic_sp,Y_tic_sp,Right,Top,X_maj_ct,Y_maj_ct,Maj_tic
2060  !GRID Xgridtic,Ygridtic,Left,Bottom,Xgridmaj,Ygridmaj,Majgrid_sz
2070  CLIP OFF
2080  CSIZE 3,.75
2090  LORG 6
2100  FOR I=Left TO Right STEP X_incmt!LABELING OF X AXIS
2110     MOVE I,(Bottom-.04*(Top))
2120     LABEL USING X_char$;I/1.E-6
2130  NEXT I
2140  LORG 8
2150  FOR I=Bottom TO Top STEP Y_incmt!LABELING OF Y AXIS
2160     MOVE (Left-.4*Tscale),I
2170     LABEL USING Y_char$;I
2180  NEXT I
2190  PENUP
2200  PEN 2
2210  LINE TYPE Line_num
2220  CLIP ON
2230  FOR I=0 TO 1023!PLOTTING OF DATA
2240     PLOT X_data(I),Y_data(I)
2250  NEXT I
2260  PENUP
2270  CLIP OFF
2280  IF A$="Y" THEN DUMP GRAPHICS #701
2290  RETURN
2300  !
2310  !*************************************************************************
2320  !            SAME GRAPH
2330  !*************************************************************************
2340  !
2350 Same_graph:  !
2360  PEN Pen_num
2370  LINE TYPE Line_num
2380  CLIP ON
```

```
2390  FOR I=0 TO 1023
2400     PLOT X_data(I),Y_data(I)
2410  NEXT I
2420  CLIP OFF
2430  PENUP
2440  RETURN
2450  !
2460  !#####################################################################
2470  !            CHANGE GRAPHICS PARAMETERS
2480  !#####################################################################
2490  !
2500 Change_params:  !
2510  OUTPUT KBD;Clear_crt$;
2520  PRINT "SELECT FROM THE FOLLOWING TO CHANGE"
2530  PRINT "CASE 1: GRAPH HEADING"
2540  PRINT "CASE 2: Y AXIS LABEL"
2550  PRINT "CASE 3: X AXIS LABEL"
2560  PRINT "CASE 4: Y AXIS UNITS"
2570  PRINT "CASE 5: X AXIS UNITS"
2580  PRINT "CASE 6: WINDOW UNITS"
2590  PRINT "CASE 7: X AXIS TICK SPACING"
2600  PRINT "CASE 8: Y AXIS TICK SPACING"
2610  PRINT "CASE 9: TICK INTVL BTWN MAJOR TICKS IN X DIRECTION"
2620  PRINT "CASE 10: TICK INTVL BTWN MAJOR TICKS IN Y DIRECTION"
2630  PRINT "CASE 11: SIZE OF MAJOR TICKS"
2640  PRINT "CASE 12: X TICK GRID SPACING"
2650  PRINT "CASE 13: Y TICK GRID SPACING"
2660  PRINT "CASE 14: GRID TICK INTVL BTWN MAJOR TICKS IN X DIRECTION"
2670  PRINT "CASE 15: GRID TICK INTVL BTWN MAJOR TICKS IN Y DIRECTION"
2680  PRINT "CASE 16: MAJOR GRID TICK SIZE"
2690  PRINT "CASE 17: Y INCREMENT"
2700  PRINT "CASE 18: X INCREMENT"
2710  PRINT "CASE 19: LINE TYPE"
2720  PRINT "CASE 20: GRAPH HEADING SUB LABEL"
2730  PRINT "CASE 21: X AXIS NUMERIC IMAGE"
2740  PRINT "CASE 22: Y AXIS NUMERIC IMAGE"
2750  !
2760  INPUT "DO YOU DESIRE TO CHANGE ANY PARAMETERS? Y=YES",Dec4$
2770  IF Dec4$="Y" THEN
2780     INPUT "ENTER PARAMETER NUMBER",Change_num
2790  ELSE
2800     GOTO 3560
2810  END IF
2820  SELECT Change_num
2830     CASE 1
2840        PRINT "CURRENT HEADING LABEL",Head_lbl$
2850        INPUT "NEW HEADING LABEL",Head_lbl$
2860     CASE 2
```

```
2870        PRINT "CURRENT Y AXIS LABEL",Y_axis_lbl$
2880        INPUT "NEW Y AXIS LABEL",Y_axis_lbl$
2890     CASE 3
2900        PRINT "CURRENT X AXIS LABEL",X_axis_lbl$
2910        INPUT "NEW X AXIS LABEL",X_axis_lbl$
2920     CASE 4
2930        PRINT "CURRENT Y AXIS UNITS",Y_axis_units$
2940        INPUT "NEW Y AXIS UNITS",Y_axis_units$
2950     CASE 5
2960        PRINT "CURRENT X AXIS UNITS",X_axis_units$
2970        INPUT "NEW X AXIS UNITS",X_axis_units$
2980     CASE 6
2990        PRINT "CURRENT WINDOW",Left,Right,Bottom,Top
3000        INPUT "NEW WINDOW",Left,Right,Bottom,Top
3010     CASE 7
3020        PRINT "CURRENT X AXIS TIC SPACING",X_tic_sp
3030        INPUT "NEW X AXIS TIC SPACING",X_tic_sp
3040     CASE 8
3050        PRINT "CURRENT Y AXIS TICK SPACING",Y_tic_sp
3060        INPUT "NEW Y AXIS TIC SPACING",Y_tic_sp
3070     CASE 9
3080        PRINT "CURRENT TIC INTVL BTWN MAJ TICS X DIR",X_maj_ct
3090        INPUT "NEW TICK INTVL BTWN MAJOR TICKS X DIR",X_maj_ct
3100     CASE 10
3110        PRINT "CURRENT TICK INTVL BTWN MAJOR TICKS Y DIR",Y_maj_ct
3120        INPUT "NEW TICK INTVL BTWN MAJOR TICKS Y DIR",Y_maj_ct
3130     CASE 11
3140        PRINT "CURRENT MAJOR TICK SIZE",Maj_tic
3150        INPUT "NEW MAJOR TICK SIZE",Maj_tic
3160     CASE 12
3170        PRINT "CURRENT X TICK GRID SPACING",X_grid_tic
3180        INPUT "NEW X TICK GRID SPACING",X_grid_tic
3190     CASE 13
3200        PRINT "CURRENT Y TICK GRID SPACING",Y_grid_tic
3210        INPUT "NEW Y TICK GRID SPACING",Y_grid_tic
3220     CASE 14
3230        PRINT "CURRENT GRID TIC INTVL BTWN MAJ TICS X DIR",X_grid_maj
3240        INPUT "NEW GRID TIC INTVL BTWN MAJ TIC X DIR",X_grid_maj
3250     CASE 15
3260        PRINT "CURRENT GRID TIC INTVL BTWN MAJ TICS Y DIR",Y_grid_maj
3270        INPUT "NEW GRID TIC INTVL BTWN MAJ TIC Y DIR",Y_grid_maj
3280     CASE 16
3290        PRINT "CURRENT MAJOR TICK SIZE",Maj_grid_sz
3300        INPUT "NEW MAJOR TICK SIZE",Maj_grid_sz
3310     CASE 17
3320        PRINT "CURRENT Y INCREMENT",Y_incmt
3330        INPUT "NEW Y INCREMENT",Y_incmt
3340     CASE 18
```

```
3350         PRINT "CURRENT X INCREMENT",X_incmt
3360         PRINT "NEW X INCREMENT",X_incmt
3370      CASE 19
3380         PRINT "CURRENT LINE TYPE",Line_num
3390         DISP "NEW LINE TYPE(1=SOLID,4=DASH,5=BIG DASH,6=DASH-DOT";
3391         INPUT Line_num
3400      CASE 20
3410         PRINT "CURRENT HEADING SUB LABEL",Sub_head_lbl$
3420         INPUT "NEW HEADING SUB LABEL",Sub_head_lbl$
3430      CASE 21
3440         PRINT "CURRENT X AXIS NUMERIC IMAGE",X_char$
3450         INPUT "NEW X AXIS NUMERIC IMAGE",X_char$
3460      CASE 22
3470         PRINT "CURRENT Y AXIS NUMERIC IMAGE",Y_char$
3480         INPUT "NEW Y AXIS NUMERIC IMAGE",Y_char$
3490   END SELECT
3500   INPUT "DO YOU WISH TO CHANGE ANOTHER PARAMETER? Y=YES",Dec5$
3510   IF Dec5$="Y" THEN
3520      GOTO 2510
3530   ELSE
3540      GOSUB Plot_data
3550   END IF
3560   RETURN
3570   !
3580   !##########################################################################
3590   !          END THE PROGRAM
3600   !##########################################################################
3610   !
3620 End_program:  !
3630   GRAPHICS OFF
3640   PRINT "END OF PROGRAM"
3650   END
```

LIST OF REFERENCES

1. Urick, Robert J., Principles of Underwater Sound, 3rd edition, McGraw-Hill, 1983.

2 Kinsler, Lawrence E., Frey, Austin R., Coppens, Alan B., and Sanders, James V., Fundamentals of Acoustics, John Wiley and Sons, 1982.

3. Crispin Jr., J. W., Siegel, K. M., Methods of Radar Cross-Section Analysis, Academic Press, 1968.

4. Harvey, Lawrence M., Application of the Sonar Equations to Bistatic Echo-Ranging, M.S. Thesis, Naval Postgraduate School, Monterey, California, March 1982.

5. Hampton, L. D., and McKinney, C. M., "Experimental Study of the Scattering of Acoustic Energy from Solid Metal Spheres in Water", The Journal of the Acoustical Society of America, Vol. 33, No. 5, pp. 664-673, May 1961.

6. Hickling, Robert, "Analysis of Echoes from a Solid Elastic Sphere in Water", The Journal of the Acoustical Society of America, Vol. 34, No. 10, pp. 1582-1592, October 1962.

7. Neubauer, Werner G., Vogt, Richard H., and Dragonette, Louis, R., "Acoustic Reflection from Elastic Spheres", The Journal of the Acoustical Society of America, Vol. 55, No. 6, pp. 1123-1137, June 1974.

8. Izbicki, J. L, Maze, G., and Ripoche, J., "Influence of the the Free Modes of Vibration on the Acoutic Scattering of a Circular Cylindrical Shell", The Journal of the Acoustical Society of America, Vol. 80, No. 4, pp. 1215-1219, October 1986.

9. Young, Joel W., Effective Target Strength, Energy Splitting Loss, and other Processor-Dependent Target Strength Metrics, BBN Laboratories, Proceedings from 1986 Symposium of Navy Underwater Acoustics.

10. Underwater Electroacoustic Standard Transducer Catalog, Naval Research Laboratory, Orlando, Florida, May 1982.

11. Faran Jr., James J., "Sound Scattering by Solid Cylinders and Spheres", The Journal of the Acoustical Society of America, Vol. 23, No. 4, pp. 405-418, July 1951.

12. Varadan, V. K., Varadan, V. V., Su, J. H., and Pillai, T. A. K., "Comparison of Sound Scattering by Rigid and Elastic Obstacles in Water", The Journal of the Acoustical Society of America, Vol. 71, No. 6, pp. 1377-1383, June 1982.

13. Tsui, Chung V., Reid, Glenn N., and Gaunaurd, Guillermo C., "Resonance Scattering by Elastic Cylinders and their Experimental Verification", The Jounal of the Acoustical Society of America, Vol. 80, No. 2, pp. 382-390, August 1986.

14. Tsui, Chung Y., Reid, Glenn N., and Gaunaurd, Guillermo C., "Bistatic Measurement of Target Scattering at Resonance", The Journal of the Acoustical Society of America, Vol. 83, No. 5, pp. 1946-1951, May 1988.

15. Personal Interview with Alan B. Coppens and James V. Sanders, Naval Postgraduate School, Monterey, California, August 1988.

16. Junger, M. C. and Feit, D., Sound, Structures, and Their Interactions, 2nd edition, MIT Press, 1986.

17. Morse, Phillip M. and Ingard, K. Uno, Theoretical Acoustics, McGraw-Hill, 1968.

18. Medwin, Herman and Clay, Clarence S., Acoustical Oceanography: Principles and Applications, John Wiley and Sons, 1977.

INITIAL DISTRIBUTION LIST

	No. Copies
1. Defense Technical Information Center Cameron Station Alexandria, Virginia 22304-6145	2
2. Library, Code 0142 Naval Postgraduate School Monterey, California 93943-5002	2
3. Commanding Officer Naval Underwater Systems Command ATTN: R. Radlinski (Code 332) New London, Connecticut 06320	1
4. Commander, Naval Sea Systems Command ATTN: PMS-417C (J. Butler) Washington, D.C. 20362	1
5. Professor J. V. Sanders, Code 61Sd Department of Physics Naval Postgraduate School Monterey, California 93943	2
6. Professor A. B. Coppens, Code 61Cz Department of Physics Naval Postgraduate School Monterey, California 93943	2
7. Professor S. L. Garrett, Code 61Gx Department of Physics Naval Postgraduate School Monterey, California 93943	1
8. Professor O. B. Wilson, Code 61Wd Department of Physics Naval Postgraduate School Monterey, California 93943	1

9. Professor K. E. Woehler, Code 61Wh 1
Department of Physics
Naval Postgraduate School
Monterey, California 93943